Research Square

Preprints are preliminary reports that have not undergone peer review.
They should not be considered conclusive, used to inform clinical practice,
or referenced by the media as validated information.

Event-Triggered Practical Predefined-Time Fault-Tolerant Synchronization of Second-Order Chaotic Systems

Xinxin Zhuang

zhuangxinxin@sdxiehe.edu.cn

Shandong Xiehe University

Wentao Qin

Shandong Xiehe University

An Yan

Shandong Xiehe University

Huikun Hao

Shandong Xiehe University

Article

Keywords:

Posted Date: November 5th, 2026

DOI: https://doi.org/10.21203/rs.3.rs-11218189/v1

License: This work is licensed under a Creative Commons Attribution 4.0 International License.
Read Full License

Additional Declarations: No competing interests reported.

Event-Triggered Practical Predefined-Time Fault-Tolerant Synchronization of Second-Order Chaotic Systems

Xinxin Zhuang[1,*,+], Wentao Qin[1,+], An Yan[1,+], and Huikun Hao[1,+]

[1]School of Engineering Science, Shandong Xiehe University, Jinan, 250107, China
[*]corresponding: zhuangxinxin@sdxiehe.edu.cn
[+]these authors contributed equally to this work

ABSTRACT

This study addresses the synchronization problem of second-order chaotic systems subject to parameter uncertainties, external disturbances, and actuator faults, and proposes a predefined-time nonsingular terminal sliding mode control (NTSMC) strategy. A nonsingular terminal sliding surface is designed so that the convergence time can be prescribed in advance. A time-varying barrier-function-based adaptive gain is developed to increase the robust gain as the sliding variable approaches the barrier boundary. The proposed strategy does not require prior knowledge of the disturbance upper bound, thereby avoiding control-gain overestimation associated with conventional fixed-gain or adaptive-gain approaches. In addition, a periodic event-triggering mechanism (ETM) is designed to transmit a new command only when the deviation of the nominal compensation command from its held value exceeds a threshold, thereby reducing the communication burden. The stability of the closed-loop system is established using Lyapunov theory. Finally, several simulation experiments demonstrate the feasibility and superior performance of the proposed scheme.

1 Introduction

Chaotic systems are widely used in control engineering[1], economics[2], image security[3], and secure communications[4]. These systems exhibit three main characteristics: complexity, unpredictability, and aperiodicity[5]. Sensitivity to initial conditions is another typical characteristic of chaotic systems. Small changes in the initial state may cause a sudden transition from one attractor to another, leading to undesirable states[6]. Therefore, chaos control is essential in practical applications. Synchronization of chaotic systems has attracted considerable attention in the field of chaos control. Representative studies include chaos control of pendulum systems[7] and synchronization of Duffing oscillators[8], Φ^6 Duffing oscillators[9], and horizontal platform systems[10].

Various methods have been proposed for chaotic system synchronization, including fuzzy control[11], robust control[12], backstepping control[13], neural network control[14], and sliding mode control (SMC)[15]. Owing to its fast response, good transient performance, ease of implementation, and strong robustness against external disturbances and system uncertainties, SMC has been widely applied to chaotic system synchronization[16]. In[4], a predefined-time sliding mode controller is proposed to guarantee synchronization of a hyperchaotic master–slave system within a predefined time. In[5], a predefined-time sliding mode controller is designed to ensure that the errors between the drive and response systems converge to the origin simultaneously within a predefined time. In[17], a norm-based adaptive gain is combined with practical predefined-time SMC for the synchronization of uncertain chaotic systems. An exponential function is incorporated into the sliding surface in[18] to achieve predefined-time synchronization of a hyperchaotic system containing a memristor. In[19], adaptive predefined-time stability conditions are established, and a sliding mode controller is designed for the synchronization of chaotic systems subject to uncertainties and external disturbances. A predefined-time sliding mode synchronization scheme is developed in[20] for a multiscroll chaotic system constructed with a single memristor. In[21], a radial basis function (RBF) neural network is combined with fixed-time SMC to achieve attitude synchronization and anti-synchronization of identical and nonidentical chaotic satellites with unknown dynamics. However, the above studies do not consider the synchronization of second-order chaotic systems subject to actuator faults.

Actuator faults cause the actual input to deviate from the desired control command and affect synchronization accuracy together with model uncertainties and external disturbances. This problem has therefore attracted considerable attention from researchers. Fault-tolerant control (FTC) is generally classified into active and passive approaches. Active FTC uses online fault detection or estimation results to adjust the control law and provide compensation, thereby helping restore control accuracy after a fault and accommodate variations in the fault[22]. Passive FTC generally employs a robust controller with a

fixed structure designed for a predefined range of faults. Its fault-tolerant capability is limited by the fault set considered in the design, and it may be highly conservative when unexpected faults occur[23]. Therefore, active FTC based on fault estimation and online compensation is an important research direction for improving control performance after faults occur. In[24], an adaptive technique is employed to approximate unknown parameters, and a new piecewise function method is proposed to address the singularity issue arising in the derivation of the virtual controller. In[25], a novel predefined-time approach is proposed to address the complex tracking problem of uncertain Euler–Lagrange systems with potential actuator faults. Fixed-time fault detection, isolation, and estimation are combined with control reconfiguration in[26] to handle intermittent faults and input saturation. In[27], nonlinear moving horizon estimation and model predictive control are used to compensate online for actuator bias and model mismatch in autonomous vehicles. A predefined-time observer is employed in[28] to estimate faults and disturbances, and compensation is implemented under full-state constraints. In[29], a predefined-time extended state observer is used to estimate lumped disturbances that include actuator faults. In[30], fault detection and indirect fault estimation are used to trigger controller switching for active FTC of spacecraft. The actuator effectiveness coefficients of robotic manipulators are estimated online in[31], and their effects are compensated for to achieve fixed-time trajectory tracking. In[32], fault detection based on an extended Kalman filter is combined with adaptive fault estimation to achieve fixed-time FTC. However, the above studies do not address how to save communication resources while guaranteeing synchronization performance in the design of fault-tolerant controllers.

An ETM determines whether an update is required according to changes in the error or control command, thereby reducing redundant communication associated with periodic transmissions. In[33], an adaptive backstepping approach is used to design an event-triggered controller that achieves predefined-time anti-synchronization of unified chaotic systems while saving communication resources. In[34], continuous and periodic ETMs are incorporated into the corresponding SMC schemes for path following of underactuated surface vehicles. Furthermore, event-triggered control is combined with nonsingular terminal SMC in[35], and event-triggered SMC for uncertain systems subject to multiple disturbances is investigated in[36]. In[37], a digital redesign approach incorporating a dynamic signal generator is employed to improve the control behavior between events. A barrier function is used in[38] to adjust the nonsingular terminal sliding mode gain. In[39], practical predefined-time sliding mode tracking is achieved through adaptive estimation. In[40], a barrier-function-based adaptive gain is further employed to reduce control updates while maintaining disturbance rejection performance. However, the above studies do not address how to ensure that the position and velocity errors of second-order chaotic systems enter prescribed neighborhoods within a predefined total time under the combined effects of actuator faults and command-holding errors.

Inspired by the above studies, this paper proposes a predefined-time NTSMC strategy for the synchronization of second-order chaotic systems subject to parametric uncertainties, external disturbances, and actuator faults. The proposed method guarantees convergence within a predefined time, maintains robustness against external disturbances and actuator faults, and saves communication resources without requiring prior knowledge of the upper bound of the lumped disturbance. The main contributions of this paper are summarized as follows:

- A regularized nonsingular sliding surface is constructed, and the relationship between the width of the sliding band and the prescribed neighborhoods of the position and velocity errors is established. By allocating time to the two stages, the synchronization errors are guaranteed to enter the prescribed neighborhoods within the predefined total time.
- An ETM is proposed and combined with continuous local feedback at the actuator side. The command-holding error is incorporated into the closed-loop analysis, and a positive lower bound on the inter-event interval is established based on the checking period, reducing unnecessary command updates.
- A barrier function is employed to compensate for the effects of faults and disturbances without requiring prior knowledge of the upper bound of the lumped disturbance, thereby avoiding the gain mismatch problem.

The remainder of this paper is organized as follows. Section 2 introduces the second-order chaotic systems, the actuator fault and disturbance models, and the preliminaries. Section 3 presents the predefined-time nonsingular terminal sliding mode controller and the stability proof. Section 4 provides comparative simulations and an analysis of the results. Section 5 concludes this paper.

2 System description and preliminaries

This section presents the master–slave synchronization model in the presence of system uncertainties, external disturbances, and actuator faults. The disturbance assumption and the preliminaries are then introduced to formulate the control objective.

2.1 System description

Consider the following class of second-order chaotic systems[1]:

$$\begin{aligned}\dot{x}_1(t) &= x_2(t),\\ \dot{x}_2(t) &= -ax_1(t) - bx_2(t) + f_1(x_1(t)) + f_2(x_2(t)) + (p + q\sin\omega_1 t)g(x_1(t)) + \tau\cos\omega_2 t,\end{aligned} \tag{1}$$

where x_1 and x_2 denote the system states, and a, b, p are model parameters. The parameters q and τ are excitation amplitudes, while $\omega_1, \omega_2 > 0$ denote the corresponding frequencies. The known nonlinear functions f_1, f_2, and g are continuously differentiable on a neighborhood of the operating region. By selecting these functions and parameters, system (1) describes several typical chaotic oscillators, as follows:

(i) A parametrically excited pendulum[7]:

$$\dot{x}_1 = x_2, \qquad \dot{x}_2 = -bx_2 - (1 + q\sin\omega t)\sin x_1, \tag{2}$$

with $q = 2$, $b = 1/10$, and $\omega = 2$.

(ii) A Duffing oscillator under harmonic excitation[8]:

$$\dot{x}_1 = x_2, \qquad \dot{x}_2 = -bx_2 - x_1^3 + (1 + q\sin\omega t)x_1, \tag{3}$$

with $q = 1/2$, $b = 1/5$, and $\omega = 1$.

(iii) A Φ^6 Duffing oscillator[9]:

$$\dot{x}_1 = x_2, \qquad \dot{x}_2 = -ax_1 - bx_2 - cx_1^3 - d_5x_1^5 + \tau\cos\omega t, \tag{4}$$

with $a = 1$, $b = 1/100$, $c = -0.495$, $d_5 = 1/20$, $\tau = 0.78$, and $\omega = 0.55$.

(iv) A non-autonomous horizontal platform system[10]:

$$\dot{x}_1 = x_2, \qquad \dot{x}_2 = -bx_2 - \lambda\sin x_1 + \mu\sin x_1\cos x_1 + \tau\cos\omega t, \tag{5}$$

with $b = 4/3$, $\lambda = 3.776$, $\mu = 4.6\times10^{-6}$, $\tau = 34/3$, and $\omega = 1.8$.

Based on (1), the master system is described by

$$\begin{aligned}\dot{x}_{m1} &= x_{m2},\\ \dot{x}_{m2} &= -ax_{m1} - bx_{m2} + f_1(x_{m1}) + f_2(x_{m2}) + (p + q\sin\omega_1 t)g(x_{m1}) + \tau\cos\omega_2 t,\end{aligned} \tag{6}$$

and the slave system subject to uncertainties and external disturbances is given by

$$\begin{aligned}\dot{x}_{s1} &= x_{s2},\\ \dot{x}_{s2} &= -ax_{s1} - bx_{s2} + f_1(x_{s1}) + f_2(x_{s2})\\ &\quad + (p + q\sin\omega_1 t)g(x_{s1}) + \tau\cos\omega_2 t\\ &\quad + \Delta(x_{s1}, x_{s2}) + \delta(t) + u_a(t),\end{aligned} \tag{7}$$

where $x_m = (x_{m1}, x_{m2})^\top$ and $x_s = (x_{s1}, x_{s2})^\top$ denote the master and slave states, respectively. The terms Δ and δ represent the system uncertainty and external disturbance, while u_a denotes the actual actuator input. These uncertain effects are collected in $d(t) = \Delta(x_{s1}(t), x_{s2}(t)) + \delta(t)$. Define the synchronization errors as

$$e_i(t) = x_{si}(t) - x_{mi}(t), \qquad i = 1, 2. \tag{8}$$

Subtracting (6) from (7) yields

$$\begin{aligned}\dot{e}_1 &= e_2, \qquad \dot{e}_2 = F(x_m, x_s, t) + u_a + d,\\ F(x_m, x_s, t) &= -ae_1 - be_2 + f_1(x_{s1}) - f_1(x_{m1}) + f_2(x_{s2}) - f_2(x_{m2})\\ &\quad + (p + q\sin\omega_1 t)\big[g(x_{s1}) - g(x_{m1})\big].\end{aligned} \tag{9}$$

Here, F collects the known differences between the master and slave dynamics. To account for actuator faults, write the actual input as $u_a = u + f_a$, where u is the commanded input and f_a denotes the fault contribution. For a loss of actuator effectiveness, $u_a = \rho(t)u$ and $f_a = (\rho(t)-1)u$, with $\rho(t)$ denoting the effectiveness factor. Combining the uncertainty, disturbance, and fault terms gives the lumped perturbation $\Delta_f = d + f_a$. Accordingly, the synchronization error system can be expressed as

$$\dot{e}_1 = e_2, \qquad \dot{e}_2 = F(x_m, x_s, t) + u + \Delta_f(t). \tag{10}$$

The following assumption is introduced for the subsequent controller design and stability analysis.

Assumption 1. *The master trajectory is bounded, and the nominal dynamics are continuously differentiable on bounded state sets, uniformly in time. The lumped perturbation Δ_f in (10) is measurable and satisfies*

$$|\Delta_f(t)| \le \bar{\Delta}_f, \qquad t \ge 0. \tag{11}$$

Here, $\bar{\Delta}_f > 0$ is a finite constant whose value is unknown to the controller.

FTC designs with fixed robust gains rely on an available upper bound of the lumped disturbance to select the gains. However, determining this bound can be difficult when actuator faults change the control effectiveness. Overestimating the bound can increase the control effort and chattering, whereas an insufficient gain may fail to compensate for the perturbation. To address this issue, the proposed controller determines its robust gain directly from a time-varying barrier function of the sliding variable.

The barrier boundary is initialized using the measured synchronization errors and contracts to a prescribed radius within a selected time. The resulting gain increases as the sliding variable approaches this boundary, providing the corrective action required to compensate for the unknown perturbation.

Furthermore, transmitting the nominal command at every checking instant consumes communication resources even when the command changes only slightly. To avoid these redundant transmissions, a periodic ETM is introduced between the controller and actuator. A new nominal command is transmitted when its deviation from the held value exceeds a prescribed threshold. Between transmissions, the actuator retains the last received nominal command, while the local sliding-mode feedback responds continuously to the current synchronization errors. This arrangement reduces redundant nominal-command transmissions while maintaining the barrier action required for predefined-time synchronization.

Remark 1. Assumption 1 constrains the magnitude of the lumped perturbation, while its upper bound is not required for gain selection. Moreover, no bound on the derivative of Δ_f is imposed. From a physical perspective, this permits bounded abrupt changes caused by actuator faults without requiring a prescribed rate of fault evolution. For loss-of-effectiveness faults, the quantity bounded by (11) is $\Delta_f = d + (\rho - 1)u$. The fault magnitude and occurrence time are also unknown to the controller.

2.2 Preliminaries

In this subsection, the definition and comparison lemma used to establish predefined-time synchronization are presented. Throughout the paper, the signed-power notation is defined by $\mathrm{sig}^q(z) = |z|^q \,\mathrm{sign}(z)$ for $q > 0$.

Definition 1. For prescribed accuracies $\varepsilon_1, \varepsilon_2 > 0$, system (10) achieves practical predefined-time synchronization if its errors satisfy $|e_i(t)| \le \varepsilon_i$ for all $t \ge T^*$, $i = 1, 2$. The time bound $T^* > 0$ is selected in advance, independently of the initial errors and without knowledge of the perturbation bound.

The following comparison lemma gives an explicit time bound for entry into a prescribed neighborhood. It follows from the exponential comparison used in predefined-time sliding-mode control[41].

Lemma 1 (Predefined-time comparison)**.** *Let $y(t)$ be a nonnegative, absolutely continuous function, and let $a > 0$, $0 < p < 1$, and $T > 0$. Suppose that the inequality*

$$\dot{y} \le -\frac{1}{pT}\exp(y^p)y^{1-p} \tag{12}$$

holds almost everywhere whenever $y(t) \ge a$. Then, for $y(t_0) > a$, the time required to reach $[0, a]$ is bounded by

$$T\left[\exp(-a^p) - \exp(-y^p(t_0))\right] < T. \tag{13}$$

Once reached, the interval $[0, a]$ remains invariant under (12).

Proof. Before entry into $[0, a]$, multiplying (12) by $-py^{p-1}\exp(-y^p)$ yields $\frac{d}{dt}\exp(-y^p) \ge 1/T$. Integrating from t_0 to the first entry time gives (13). Since (12) is strictly negative whenever $y \ge a$, an outward excursion from a is excluded. Thus, the interval remains invariant after entry, which completes the proof.

□

2.3 Control objective

The control objective of this paper is to develop a barrier-function-based predefined-time NTSMC strategy for the synchronization of systems (6) and (7). In the presence of uncertainties, external disturbances, and actuator faults, both synchronization errors should enter prescribed neighborhoods of zero within a time selected in advance. The closed-loop signals should remain bounded, and nominal-command transmissions should admit a strictly positive minimum interval.

For given $T^* > 0$ and $\varepsilon_1, \varepsilon_2 > 0$, select positive time parameters T_d and T_c such that

$$T_d + T_c = T^*. \tag{14}$$

The parameter T_d specifies the time by which the sliding variable s, defined in Section 3, enters and remains in the band $|s| < \sigma$. The parameter T_c specifies the subsequent time allowed for the synchronization errors to reach their prescribed neighborhoods. The required error bounds are

$$|e_1(t)| \le \varepsilon_1, \qquad |e_2(t)| \le \varepsilon_2, \qquad t \ge T_d + T_c. \tag{15}$$

The triggering condition is checked at $t_k = kh$, where $h > 0$ is the checking period. The actuator holds the last transmitted nominal compensation and combines it with local sliding-mode feedback evaluated continuously from the available synchronization errors. Consequently, consecutive nominal-command transmissions are separated by at least h. The actuator model has no input saturation.

Remark 2. In finite-time control, the settling-time bound generally depends on the initial errors, while fixed-time control provides an initial-condition-independent bound determined by the controller parameters. Here, the total bound $T^* = T_d + T_c$ is specified directly before selecting the remaining design parameters. The prescribed time and error accuracies are therefore explicit control objectives. Their selection does not require the numerical value of $\bar{\Delta}_f$.

3 Barrier-function-based predefined-time NTSMC strategy

To achieve the control objective, a nonsingular terminal sliding variable is first constructed. A time-varying barrier function is then introduced to determine the robust gain, and a periodic ETM schedules the nominal-command transmissions. Finally, Lyapunov analysis establishes sliding-band reaching within T_d and practical synchronization within the total time $T_d + T_c$.

Figure 1 shows the flowchart of the proposed control scheme.

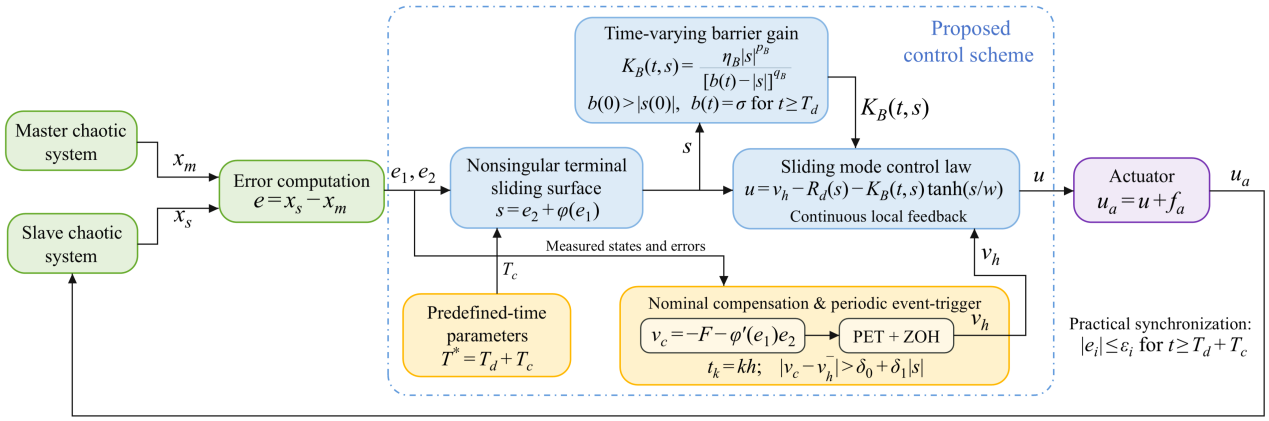


Figure 1. Flowchart of the proposed control scheme.

3.1 Nonsingular terminal sliding variable

To prescribe the error-convergence time while avoiding singular compensation near the origin, the sliding variable is designed as follows:

$$\begin{aligned} s &= e_2 + \phi(e_1), \\ \phi(z) &= \frac{\exp(|z|^n)}{n(1-\vartheta)T_c} \begin{cases} (1+n)\iota^{-n} z - n\iota^{-1-n} z|z|, & |z| \le \iota, \\ \mathrm{sig}^{1-n}(z), & |z| > \iota, \end{cases} \end{aligned} \tag{16}$$

where $0 < n < 1$, $0 < \vartheta < 1$, $T_c > 0$, and $\iota > 0$ are design parameters. The inner branch regularizes the signed-power term over $|z| \le \iota$. The resulting function ϕ is odd, strictly increasing, and continuously differentiable, with

$$\phi'(0) = \frac{(1+n)\iota^{-n}}{n(1-\vartheta)T_c} < \infty. \tag{17}$$

The two branches have matching values and first derivatives at $z = \pm\iota$. Thus, the term $\phi'(e_1)e_2$ used in the nominal compensation remains nonsingular.

To meet the prescribed synchronization accuracies, choose the error radius a_e and sliding-band radius σ to satisfy

$$\begin{aligned} 0 < \iota \le a_e \le \varepsilon_1, \qquad & 0 < \sigma \le \vartheta\phi(a_e), \\ & \sigma + \phi(a_e) \le \varepsilon_2. \end{aligned} \tag{18}$$

These conditions relate the sliding-band width to the position- and velocity-error accuracies using known design parameters. For any positive $T_c, \varepsilon_1, \varepsilon_2$, they can be satisfied by first selecting $a_e \le \varepsilon_1$ sufficiently small that

$$\frac{\exp(a_e^n)a_e^{1-n}}{n(1-\vartheta)T_c} \le \frac{\varepsilon_2}{1+\vartheta/2}, \tag{19}$$

and then choosing $0 < \iota \le a_e$ and setting $\sigma = \vartheta\phi(a_e)/2$. This construction determines the accuracy parameters without using the unknown perturbation bound.

3.2 Time-varying barrier function and controller design

To include the initial sliding variable in the barrier domain, choose $\delta_B > 0$ and set $b_0 = \sigma + |s(0)| + \delta_B$. The barrier boundary is designed to contract to σ at the prescribed time T_d:

$$b(t) = \begin{cases} \sigma + (b_0 - \sigma)(1 - t/T_d)^2, & 0 \le t < T_d, \\ \sigma, & t \ge T_d. \end{cases} \tag{20}$$

The boundary b is continuously differentiable and satisfies $b(t) \ge \sigma$ and $|s(0)| < b_0$. Its rate of change satisfies

$$|\dot{b}(t)| \le L_b := \frac{2(b_0 - \sigma)}{T_d}. \tag{21}$$

The initial error determines the starting barrier width, while the time parameters and gain parameters are selected in advance.

Within the domain $|s| < b(t)$, the robust feedback gain is defined by the following barrier function:

$$K_B(t,s) = \eta_B \frac{|s|^{p_B}}{[b(t) - |s|]^{q_B}}, \qquad \eta_B > 0, \quad 0 < p_B < 1, \quad q_B > 1. \tag{22}$$

For each fixed time, K_B is nonnegative, symmetric in s, and strictly increasing with $|s|$. Moreover, $K_B \to \infty$ as $|s| \to b(t)^-$. This property strengthens the corrective feedback as the sliding variable approaches the boundary, without requiring an estimate of $\bar{\Delta}_f$.

Based on the sliding variable (16), the nominal compensation and local reaching term are chosen as

$$\begin{aligned} v_c(t) &= -F(x_m, x_s, t) - \phi'(e_1)e_2, \\ R_d(s) &= \frac{\exp(|s|^{2m})|s|^{1-2m}}{mT_d}\tanh(s/w), \end{aligned} \tag{23}$$

where $0 < m < 1/2$ and $w > 0$, so that $sR_d(s) \ge 0$. To schedule nominal-command transmissions, the following rule is evaluated at each checking instant $t_k = kh$:

$$v_h(t_k) = \begin{cases} v_c(t_k), & k = 0 \text{ or } |v_c(t_k) - v_h(t_k^-)| > \delta_0 + \delta_1|s(t_k)|, \\ v_h(t_k^-), & \text{otherwise}, \end{cases} \tag{24}$$

where $\delta_0 > 0$ and $\delta_1 \ge 0$ determine the triggering threshold. A new nominal command is transmitted when its deviation from the held value exceeds this threshold. Otherwise, the previous value is retained, and v_h remains constant between checking instants. The control input is then constructed as

$$u(t) = v_h(t) - R_d(s(t)) - K_B(t, s(t))\tanh(s(t)/w). \tag{25}$$

The actuator combines the held nominal command with the two continuously evaluated local feedback terms in (25). The barrier feedback therefore responds to changes in s between nominal-command transmissions. The factor $\tanh(s/w)$ smooths the local switching action, with w determining the transition width around the origin.

Taking the derivative of (16) and substituting (25) into (10) yields

$$\begin{aligned} \dot{s} &= -R_d(s) - K_B(t,s)\tanh(s/w) + r_v + \Delta_f, \\ r_v &= v_h - v_c, \qquad \dot{e}_1 = -\phi(e_1) + s. \end{aligned} \tag{26}$$

Here, r_v denotes the nominal-command holding error, which enters the sliding dynamics together with the lumped perturbation.

3.3 Stability analysis

The stability analysis proceeds from the sliding-band dynamics to the synchronization errors. The state trajectories are locally absolutely continuous, and the differential inequalities hold almost everywhere. Since $\dot{e}_1 = e_2$ with continuous e_2, the derivative of $|e_1|$ exists at every nonzero error, including the boundaries considered below.

Theorem 1 (Predefined-time sliding-band reaching and barrier invariance)**.** *For system* (10) *satisfying Assumption 1, apply the sliding variable* (16) *and controller* (25) *with the transmission rule* (24)*. For every finite initial error, the barrier gain is well defined, and the synchronization errors, nominal command, barrier gain, and control input remain bounded. Furthermore, the sliding variable satisfies*

$$|s(t)| < b(t) \quad (t \geq 0), \qquad |s(t)| < \sigma \quad (t \geq T_d). \tag{27}$$

The deadline T_d is selected without knowing $\bar{\Delta}_f$.

Proof. The proof first establishes barrier invariance, then derives the reaching-time and boundedness results.

Step 1. Barrier invariance. Since ϕ is increasing and unbounded, choose $X > |e_1(0)|$ such that $\phi(X) > b_0$. Consider the solution up to a possible first exit from the domain $|e_1| < X$, $|s| < b(t)$. Within this domain,

$$|e_2| \leq b_0 + \phi(X), \qquad |v_c| \leq \bar{v} \tag{28}$$

where $\bar{v}$ is finite because the master trajectory is bounded and the nominal dynamics satisfy Assumption 1. Each transmitted value, including $v_h(0)$, is a sample of v_c taken before the possible exit. Therefore,

$$|v_h| \leq \bar{v}, \qquad |r_v| \leq 2\bar{v}, \qquad |r_v + \Delta_f| \leq C := 2\bar{v} + \bar{\Delta}_f. \tag{29}$$

The constant C bounds the combined effect of the holding error and lumped perturbation.

Choose the Lyapunov function $V_s = s^2/2$. Taking its derivative along (26) gives

$$\begin{aligned} \dot{V}_s &= -sR_d(s) - |s|K_B(t,s)|\tanh(s/w)| + s(r_v + \Delta_f) \\ &\leq -sR_d(s) - |s|\big[K_B(t,s)|\tanh(s/w)| - C\big]. \end{aligned} \tag{30}$$

To account for the contracting boundary, introduce $z = s/b(t)$, $q = |z|$, and the normalized Lyapunov function $W = z^2/2$. Its derivative satisfies

$$\dot{W} \leq -\frac{q}{b(t)}\big[K_B(t,s)|\tanh(s/w)| - C - L_b\big]. \tag{31}$$

where $sR_d(s) \geq 0$, $q \leq 1$, and $|\dot{b}| \leq L_b$ have been used. Since $\sigma \leq b(t) \leq b_0$, the barrier feedback satisfies

$$\begin{aligned} K_B(t,s)|\tanh(s/w)| &\geq H(q), \\ H(q) &= \kappa_B \frac{q^{p_B}}{(1-q)^{q_B}}\tanh(\sigma q/w), \\ \kappa_B &= \eta_B \min\{\sigma^{p_B-q_B}, b_0^{p_B-q_B}\} > 0. \end{aligned} \tag{32}$$

The function H is strictly increasing and tends to infinity as $q \to 1^-$. Hence, there exists $q_* \in (|s(0)|/b_0, 1)$ such that

$$H(q_*) > C + L_b. \tag{33}$$

For $q \geq q_*$, inequality (31) gives $\dot{W} < 0$, which prevents q from crossing q_*. At the boundary $|e_1| = X$, the error dynamics also give

$$\frac{d}{dt}|e_1| \leq -\phi(X) + b_0 < 0. \tag{34}$$

Thus, the solution cannot exit through either boundary, and it satisfies

$$|e_1(t)| < X, \qquad |s(t)| \leq q_* b(t) < b(t) \tag{35}$$

throughout its interval of existence. The bounds in (28) therefore hold along the trajectory. Inequality (33) shows that the barrier feedback compensates for the lumped perturbation, the holding error, and the boundary contraction. The constant q_* specifies the resulting separation from the barrier boundary and is used in the analysis only.

Step 2. Predefined-time sliding-band reaching. By construction, $b(T_d) = \sigma$, and (35) gives $|s(T_d)| \leq q_* \sigma < \sigma$. For every $t \geq T_d$, the boundary remains equal to σ, so the sliding variable remains inside the prescribed band. Thus, the complete reaching phase takes no longer than T_d. The unknown perturbation affects the margin q_*, while the radius σ and reaching-time bound T_d are prescribed by the designer.

Step 3. Boundedness of the closed-loop signals. The positive gap $b(t) - |s(t)| \geq (1 - q_*)\sigma > 0$ guarantees that K_B remains bounded along the closed-loop trajectory. Equations (28) and (25) then give bounded e_2, v_h, and u. Together with the bounded master trajectory and locally regular feedback, these bounds exclude finite escape and extend the solution to all $t \geq 0$. The states e_1, e_2 and the sliding variable s remain continuous across perturbation jumps and nominal-command updates. Consequently, the differential inequalities hold almost everywhere, completing the proof. □

Theorem 2 (Practical predefined-time synchronization)**.** *Under the conditions of Theorem 1, select the accuracy parameters according to (18). Then, the synchronization errors enter and remain in the sets*

$$\Omega_1 = \{e_1 : |e_1| \leq a_e\}, \qquad \Omega_2 = \{e_2 : |e_2| \leq \sigma + \phi(a_e)\} \tag{36}$$

no later than $T_d + T_c$. Consequently, (15) holds, and practical predefined-time synchronization is achieved within the prescribed time $T^* = T_d + T_c$.

Proof. **Step 1. Predefined-time convergence of the position error.** By Theorem 1, the sliding variable satisfies $|s(t)| < \sigma$ for all $t \geq T_d$. Choose the Lyapunov function $V_e = e_1^2/2$. Its derivative along (26) satisfies

$$\dot{V}_e = -e_1\phi(e_1) + e_1 s \leq -|e_1|\big[\phi(|e_1|) - \sigma\big]. \tag{37}$$

For $|e_1| \geq a_e \geq \iota$, the monotonicity of ϕ and condition (18) give $\sigma \leq \vartheta\phi(|e_1|)$. It follows that

$$\begin{aligned} \dot{V}_e &\leq -(1-\vartheta)|e_1|\phi(|e_1|) \\ &= -\frac{1}{nT_c}\exp(|e_1|^n)|e_1|^{2-n}, \\ \frac{d}{dt}|e_1| &\leq -\frac{1}{nT_c}\exp(|e_1|^n)|e_1|^{1-n}. \end{aligned} \tag{38}$$

If $|e_1(T_d)| > a_e$, applying Lemma 1 gives the additional time required to enter Ω_1:

$$T_e \leq T_c\big[\exp(-a_e^n) - \exp(-|e_1(T_d)|^n)\big] < T_c. \tag{39}$$

If $|e_1(T_d)| \leq a_e$, take $T_e = 0$.

Step 2. Invariance of the error bounds. At the boundary $|e_1| = a_e$, inequality (37) yields

$$\frac{d}{dt}|e_1| \leq -\phi(a_e) + \sigma \leq -(1-\vartheta)\phi(a_e) < 0. \tag{40}$$

Thus, Ω_1 remains invariant after entry. Using $e_2 = s - \phi(e_1)$, the synchronization errors satisfy

$$|e_1| \leq a_e \leq \varepsilon_1, \qquad |e_2| \leq \sigma + \phi(a_e) \leq \varepsilon_2. \tag{41}$$

Combining (27) and (39) gives a total synchronization time no greater than $T_d + T_c$. The time and accuracy parameters are selected independently of the unknown perturbation bound, which completes the proof. □

Remark 3. The factor $(1-\vartheta)^{-1}$ in (16) compensates for the residual sliding variable in the error dynamics. Together with $\sigma \le \vartheta\phi(a_e)$, it preserves the error-convergence bound T_c within the band $|s| < \sigma$. For a prescribed $T^* > 0$, the time allocation can be selected as $T_d = \chi T^*$ and $T_c = (1-\chi)T^*$, where $0 < \chi < 1$. The accuracy parameters are then determined from (18), providing a direct procedure for selecting both the synchronization time and error bounds.

Theorem 3 (Exclusion of Zeno transmissions)**.** *Under the nominal-command transmission rule* (24)*, consecutive transmissions are separated by at least h. Therefore, the mechanism excludes Zeno behavior.*

Proof. Each transmission occurs at a checking instant $t_k = kh$. If consecutive transmissions correspond to indices $k_j < k_{j+1}$, their separation is $(k_{j+1}-k_j)h \ge h > 0$. Hence, at most $\lfloor T/h \rfloor + 1$ nominal commands are transmitted on any interval $[0,T]$, which excludes infinitely many transmissions in finite time. □

4 Simulation results

In this section, numerical simulations are conducted to evaluate the synchronization performance under model uncertainty, external disturbances, and actuator faults. The Duffing oscillator and the Φ^6 Duffing oscillator are considered for comparative simulations. The communication performance is then evaluated, followed by additional tests on a non-autonomous horizontal platform system with different prescribed durations.

The simulation time is 30 s, and the checking period is $h = 0.001$ s. The proposed controller uses a second-order implicit Runge–Kutta method with an internal step of 0.00005 s; the reference simulations retain the fourth-order Runge–Kutta method with a step of 0.0001 s. The evaluation grid is $\Delta t = 0.0001$ s. The simulation curves are plotted in MATLAB using the saved trajectories. The parameters of the proposed controller and triggering mechanism are listed in Table 1. For Case 2, $T_c = 0.170403$ s, $T_d = 0.151929$ s, and $\iota = 8.939156 \times 10^{-8}$; the remaining parameters are unchanged. The same Case 1 and Case 2 parameter sets are used for both oscillators. The numerical time-scale parameter is denoted by T_r.

Table 1. Parameters of the proposed controller and triggering mechanism

Parameter	Value	Parameter	Value
T_c	0.288819 s	T_d	0.257507 s
n	0.493828	m	0.130440
ι	2.533909×10^{-7}	ϑ	0.200
η_B	210.055587	σ	0.0005
p_B	0.740602	δ_0	0.001
w	85.121272	h	0.001 s
q_B	1.680310	δ_B	12.964453
ε_1	0.005	ε_2	0.005
δ_1	0.010		

For all simulations, the uncertainty and external disturbance of the slave system are selected as $\Delta = 0.2\cos(x_{s2})\sin(x_{s2})$ and $\delta(t) = 2\sin(2\pi t)$, respectively. The actuator effectiveness is given by

$$\rho(t) = \begin{cases} 1, & t < 8.13 \text{ s}, \\ 0.4, & t \ge 8.13 \text{ s}. \end{cases} \tag{42}$$

Thus, a 60% loss of actuator effectiveness occurs at 8.13 s. The disturbance, fault time, and effectiveness coefficient are unavailable to the controllers. No actuator saturation is imposed.

4.1 Comparative simulations

To assess the synchronization performance, comparative simulations are conducted with the controllers in Reference[38], Reference[39], and Reference[40]. The three controllers are implemented for the same two-state synchronization error system. Their numerical settings are provided in the accompanying simulation files. All methods are tested under the same initial conditions, uncertainties, disturbances, and actuator fault.

Two cases are considered. In Case 1, the initial states of the master and slave systems are $(x_{m1}(0), x_{m2}(0)) = (1,1)$ and $(x_{s1}(0), x_{s2}(0)) = (0.5, 0.5)$, respectively. In Case 2, the corresponding initial states are $(0.4, 0.8)$ and $(0.6, 0.4)$.

The convergence time of e_i is measured as the earliest sampled time after which $|e_i| \leq 0.005$ holds until the fault occurs. The position-error root mean square error (RMSE) is used to evaluate synchronization accuracy over the complete simulation interval:

$$\mathrm{RMSE}_1 = \sqrt{\frac{1}{N+1}\sum_{k=0}^{N} e_1^2(k\Delta t)}, \qquad N = 300000. \tag{43}$$

Both the initial transient and the fault response are included in this index. The sampled peak actual control input is calculated on the internal integration grid, with $u_a = \rho u$ for the proposed controller. Convergence times and RMSE are calculated on the common evaluation grid.

4.1.1 Duffing oscillator

First, the Duffing oscillator in (3) is considered. The system parameters are selected as $b = 0.2$, $q = 0.5$, and $\omega = 1$. Fig. 2 presents the phase trajectory with the initial state $(0.5, 0.5)$.

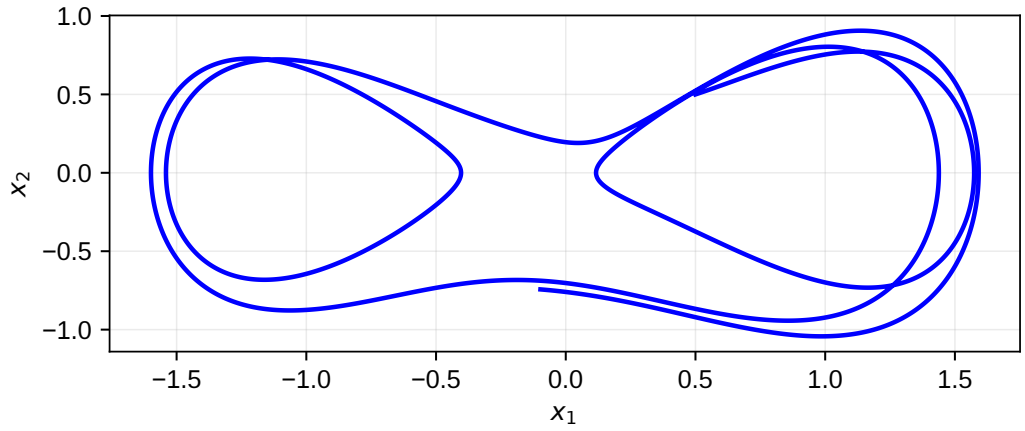


Figure 2. Phase trajectory of the Duffing oscillator.

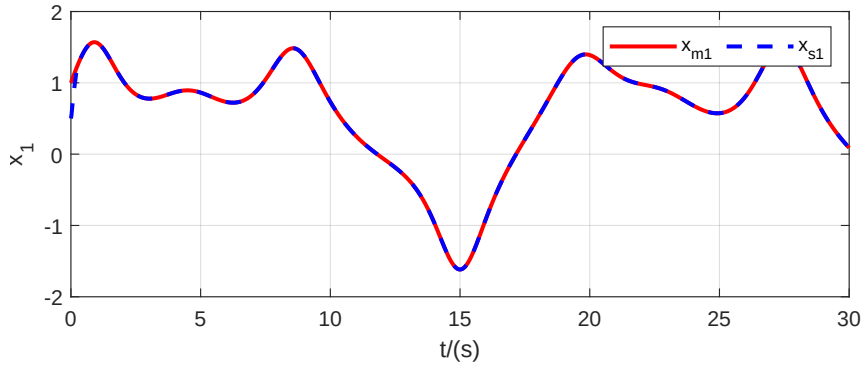
Table 2 provides a quantitative comparison for the two initial conditions. In Case 1, the convergence times of e_1 and e_2 under the proposed controller are 0.2476 s and 0.2638 s, respectively. Both are shorter than those obtained with Reference[38], Reference[39], and Reference[40]. In Case 2, the corresponding times are 0.1313 s and 0.1464 s. These results demonstrate the faster initial synchronization achieved in both cases.

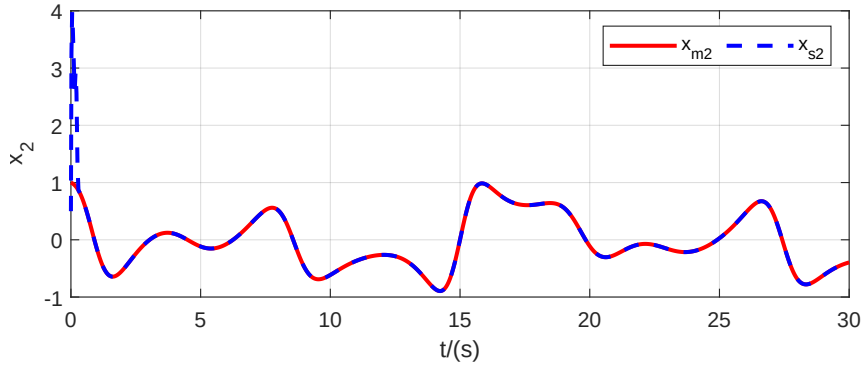
Table 2. Performance comparison for the Duffing oscillator

Metric	Proposed	Reference[38]	Reference[39]	Reference[40]
Case 1				
Convergence time of e_1 (s)	0.2476	0.4571	0.7341	0.4715
Convergence time of e_2 (s)	0.2638	0.5141	0.8453	0.6378
RMSE_1	0.0252	0.0338	0.0426	0.0339
Peak actual control input	226.78	45.44	18.55	57.33
Case 2				
Convergence time of e_1 (s)	0.1313	0.5317	0.4290	0.2874
Convergence time of e_2 (s)	0.1464	0.6034	0.5226	0.4737
RMSE_1	0.0074	0.0117	0.0119	0.0094
Peak actual control input	184.32	15.72	10.46	35.10

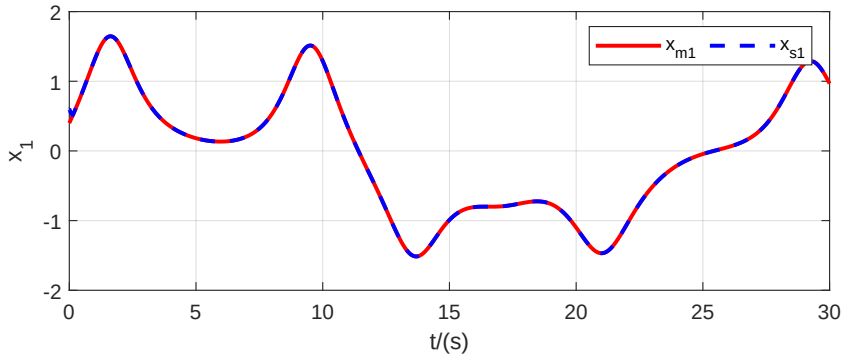
The trajectories of the master and slave systems are shown in Fig. 3. The slave states approach the master states and remain close after the actuator fault. Fig. 4 presents the synchronization error comparison. The proposed controller has the smallest position-error RMSE in both cases.

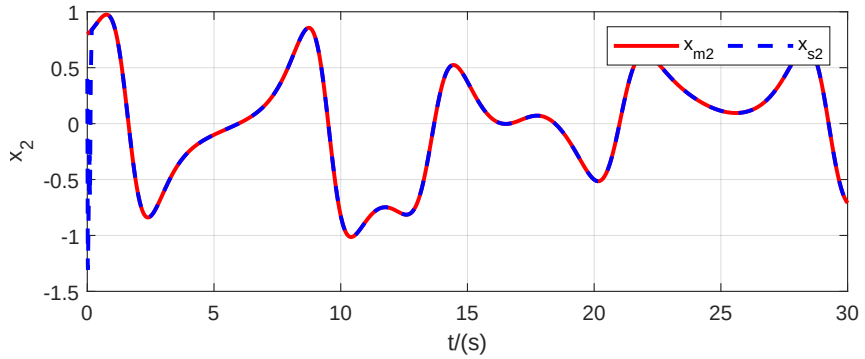
The sliding variable and actual control inputs are shown in Figs. 5 and 6, respectively. The recorded sliding variable remains within $|s| < b(t)$. The proposed controller produces a larger initial control action, with sampled peak actual inputs of 226.78





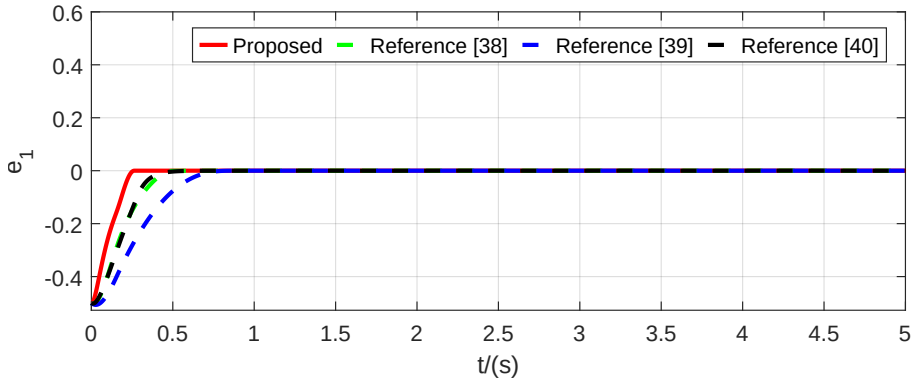
(a) Case 1

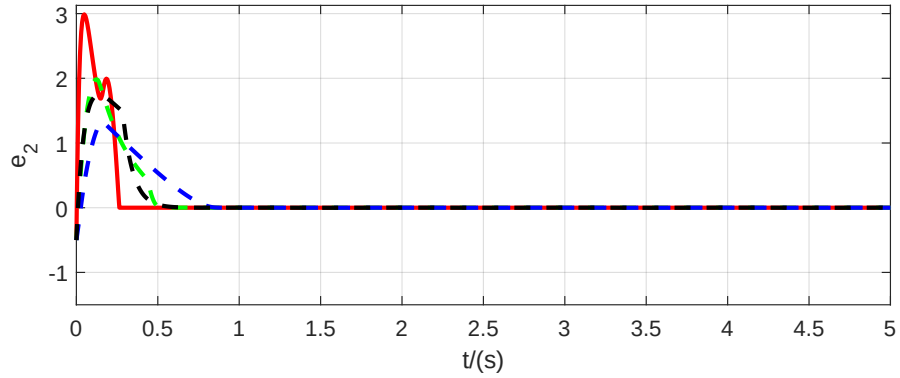




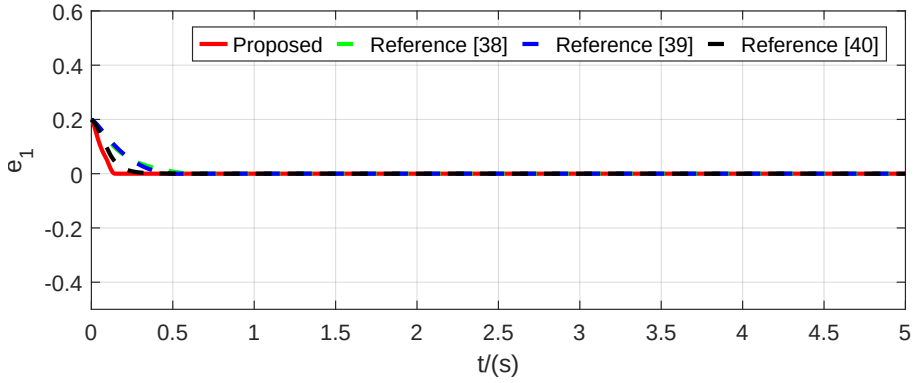
(b) Case 2

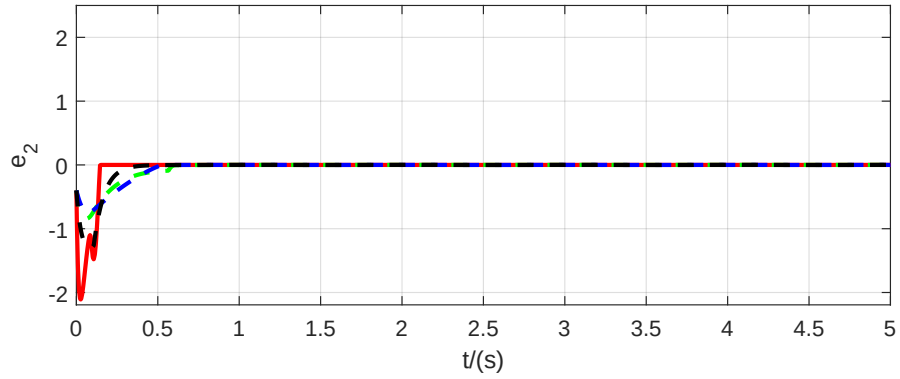
Figure 3. State trajectories of the Duffing master and slave systems.





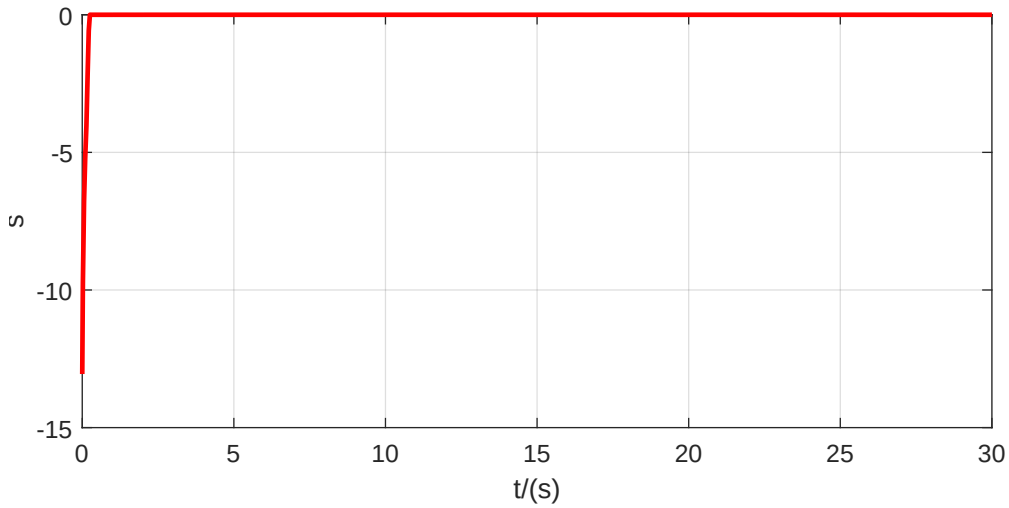
(a) Case 1



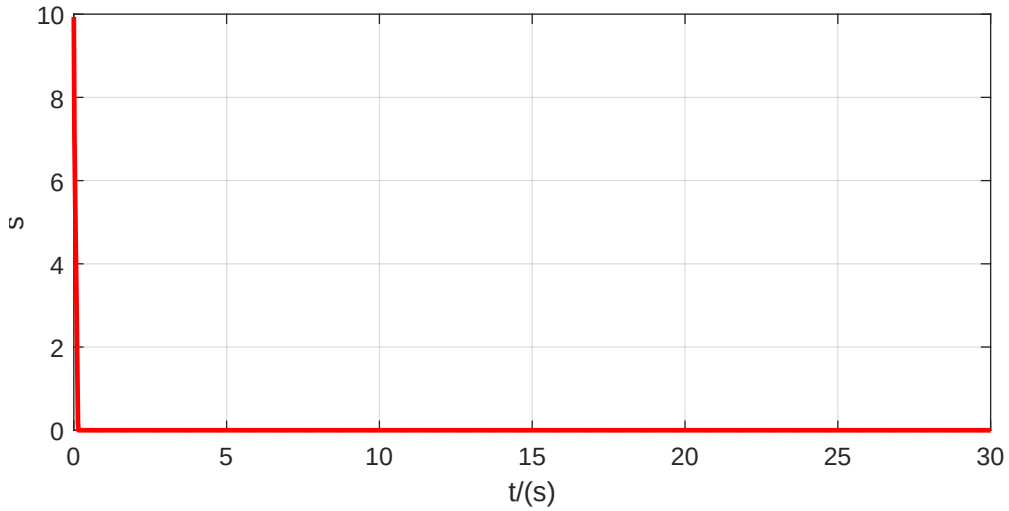


(b) Case 2

Figure 4. Synchronization error comparison for the Duffing oscillator.

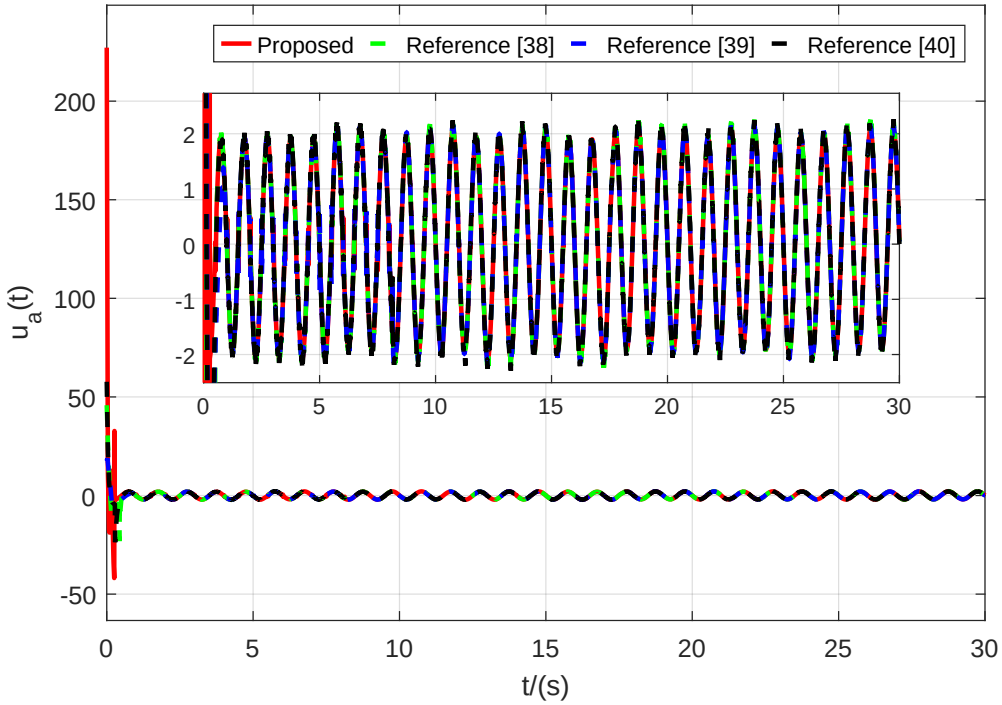


(a) Case 1

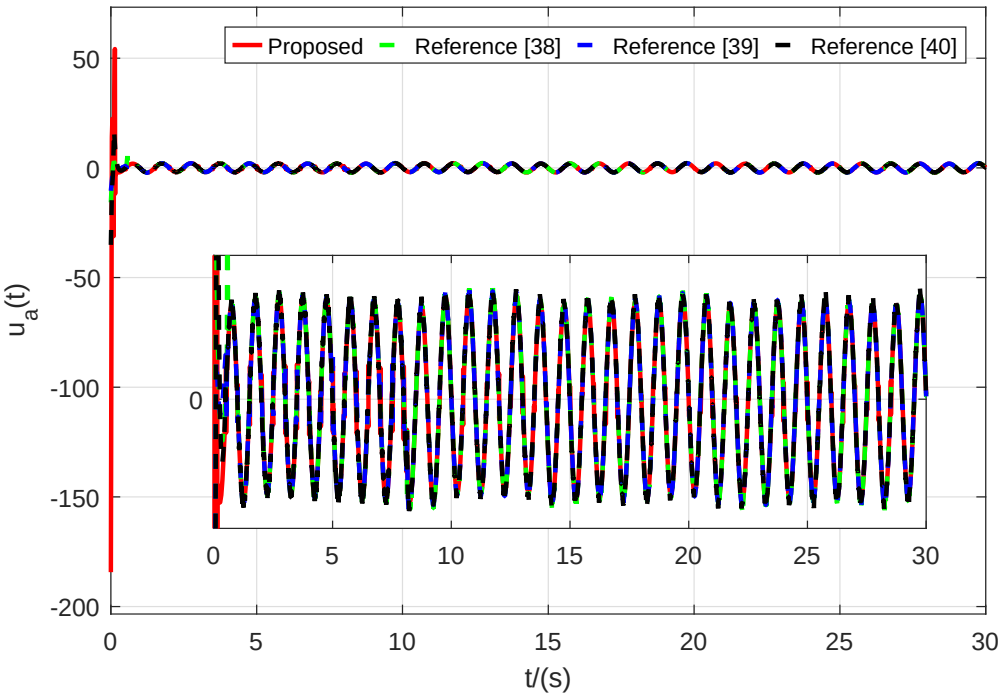


(b) Case 2

Figure 5. Sliding variable of the proposed controller for the Duffing oscillator.



(a) Case 1



(b) Case 2

Figure 6. Actual control input comparison for the Duffing oscillator.

and 184.32 in Cases 1 and 2, respectively. In Case 1, the faster transient response requires a higher peak input than the reference controllers.

4.1.2 Φ^6 Duffing oscillator

Next, the Φ^6 Duffing oscillator in (4) is selected. The system parameters are $a = 1$, $b = 0.01$, $c = -0.495$, $d_5 = 0.05$, $\tau = 0.78$, and $\omega = 0.55$, where d_5 denotes the fifth-order coefficient. The phase trajectory with the initial state $(0.5, 0.5)$ is shown in Fig. 7. The two initial conditions and controller parameters are the same as those used for the Duffing oscillator.

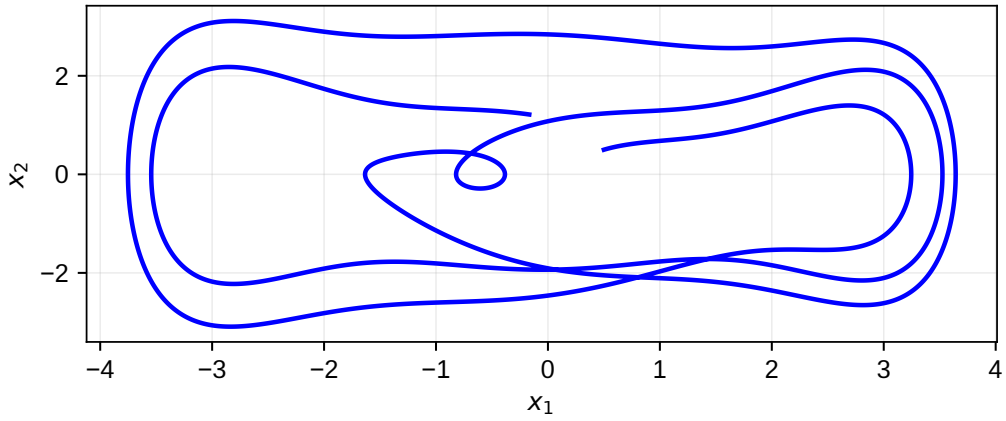


Figure 7. Phase trajectory of the Φ^6 Duffing oscillator.

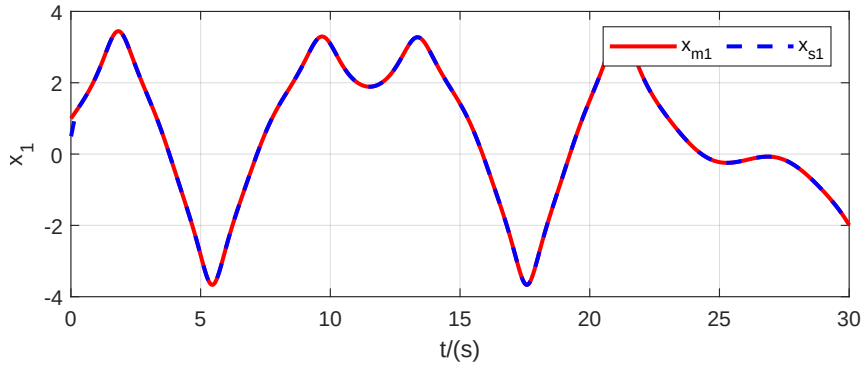
Table 3. Performance comparison for the Φ^6 Duffing oscillator

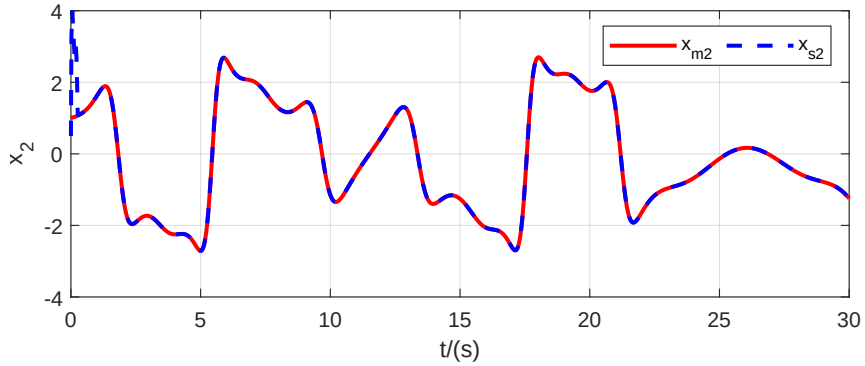
Metric	Proposed	Reference[38]	Reference[39]	Reference[40]
		Case 1		
Convergence time of e_1 (s)	0.2476	0.4578	0.7341	0.4714
Convergence time of e_2 (s)	0.2638	0.5150	0.8438	0.6379
RMSE_1	0.0252	0.0338	0.0425	0.0339
Peak actual control input	227.13	45.79	18.89	57.68
		Case 2		
Convergence time of e_1 (s)	0.1313	0.5316	0.4290	0.2874
Convergence time of e_2 (s)	0.1464	0.6033	0.5224	0.4737
RMSE_1	0.0074	0.0117	0.0119	0.0094
Peak actual control input	184.07	15.47	10.20	34.85

Table 3 presents the performance comparison. In Case 1, both errors of the proposed controller enter the prescribed tolerance band by 0.2638 s. The corresponding times are 0.5150 s, 0.8438 s, and 0.6379 s for Reference[38], Reference[39], and Reference[40], respectively. In Case 2, the proposed controller also achieves the shortest convergence times for both errors.

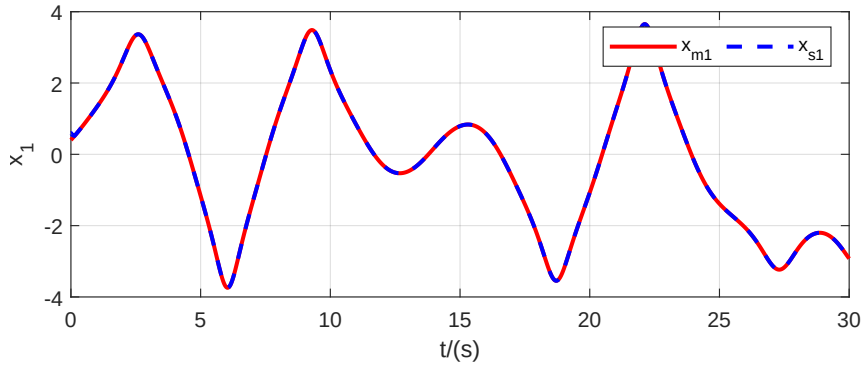
Fig. 8 shows the state trajectories, and Fig. 9 presents the synchronization errors. The slave system follows the master system under the imposed uncertainty, disturbance, and actuator fault. As in the Duffing example, the proposed controller gives the smallest position-error RMSE in both cases.

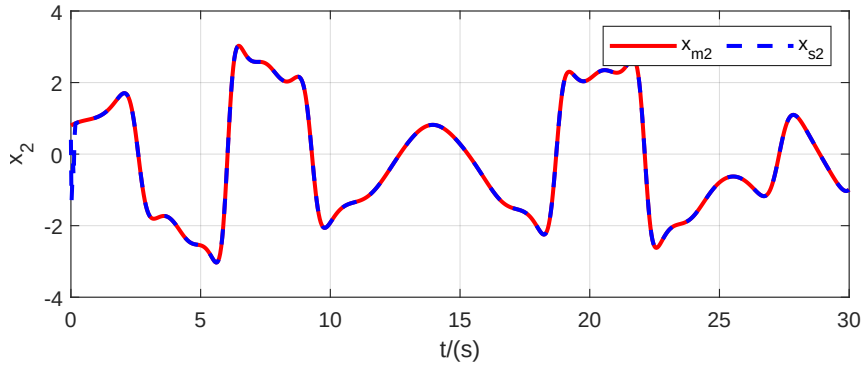
Figs. 10 and 11 show the sliding variable and actual control inputs. The sliding variable remains inside its time-varying barrier. The sampled peak actual input of the proposed controller is 227.13, compared with 45.79, 18.89, and 57.68 for Reference[38], Reference[39], and Reference[40], respectively. The results confirm the same relation between the faster initial response and the larger peak control input observed in the first example.





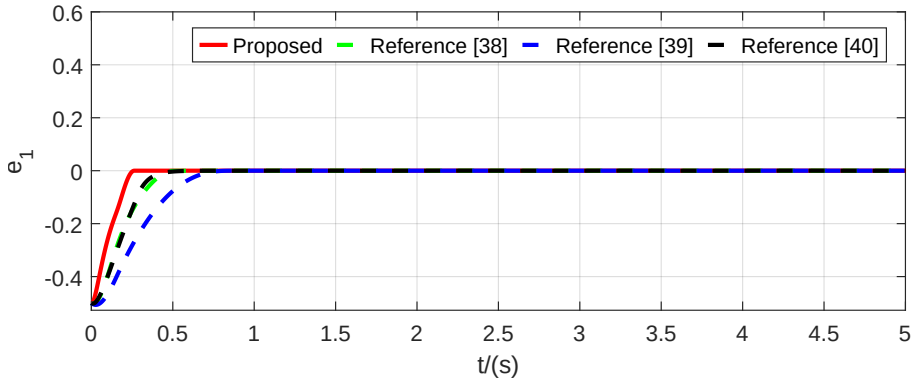
(a) Case 1

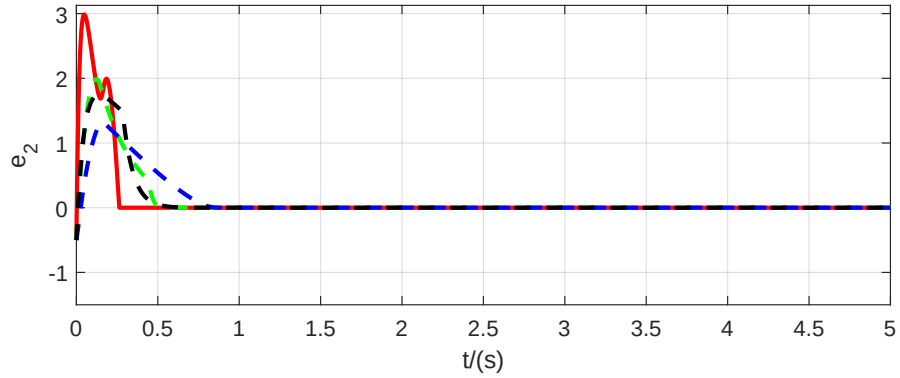




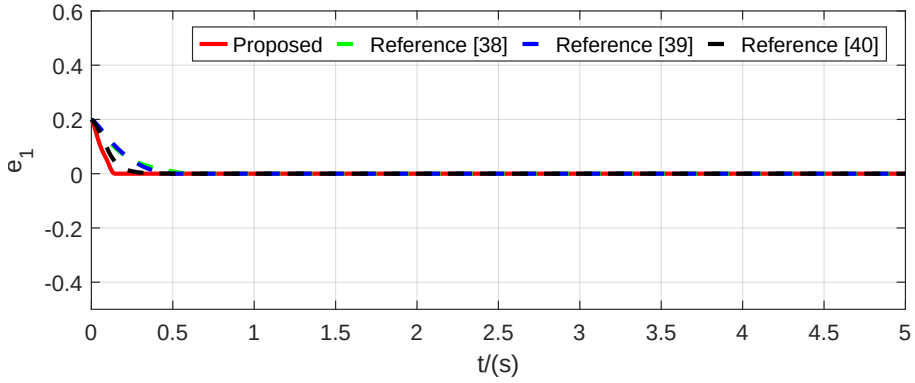
(b) Case 2

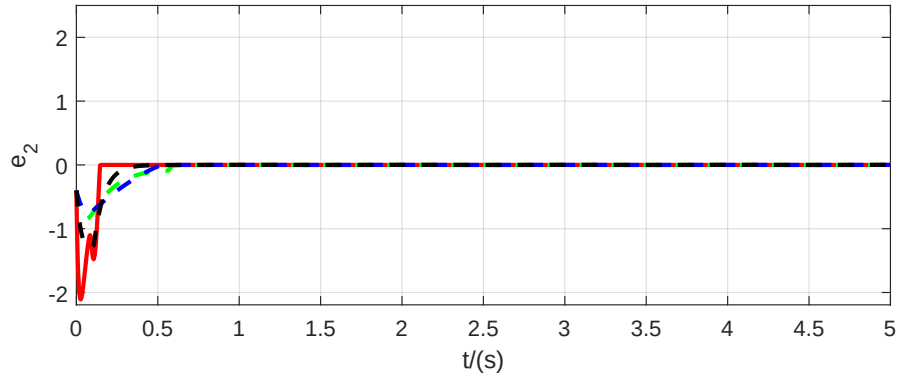
Figure 8. State trajectories of the Φ^6 Duffing master and slave systems.





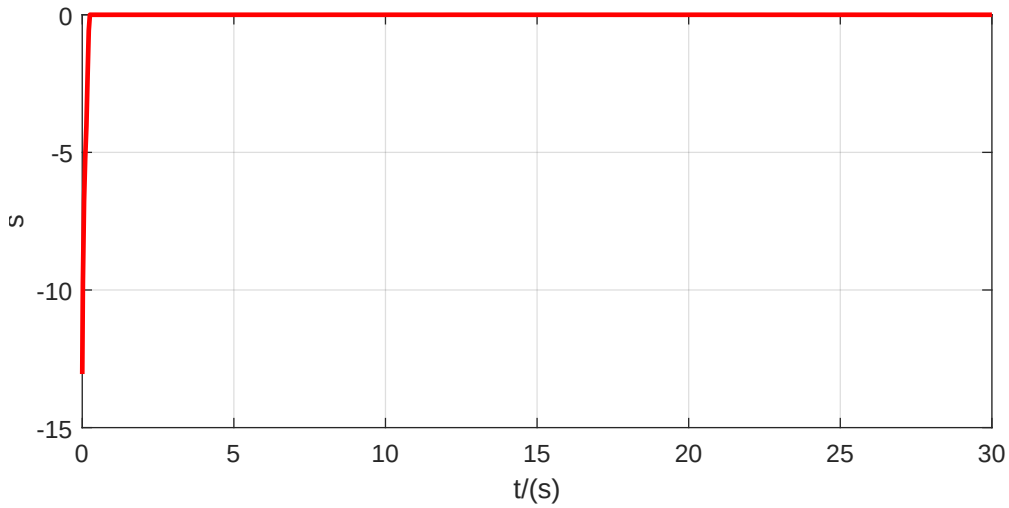
(a) Case 1



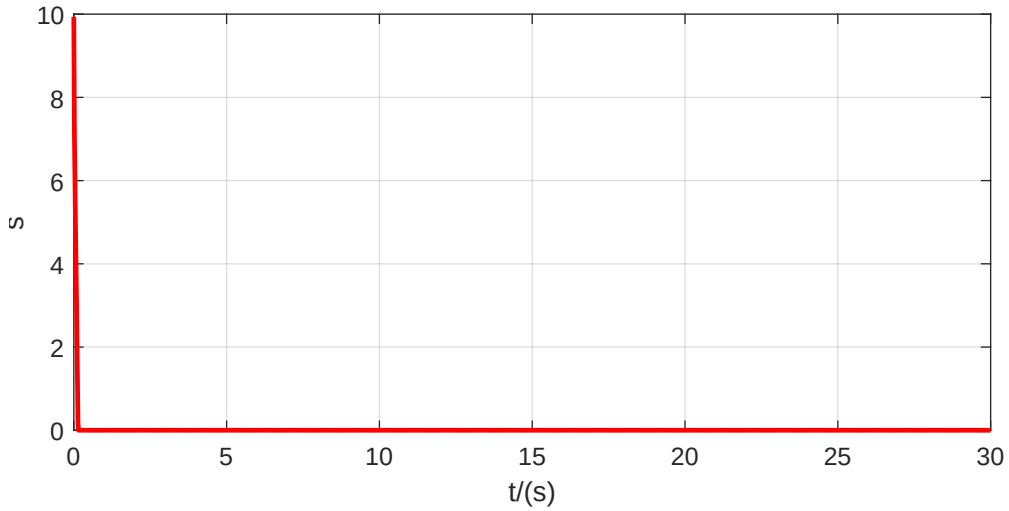


(b) Case 2

Figure 9. Synchronization error comparison for the Φ^6 Duffing oscillator.

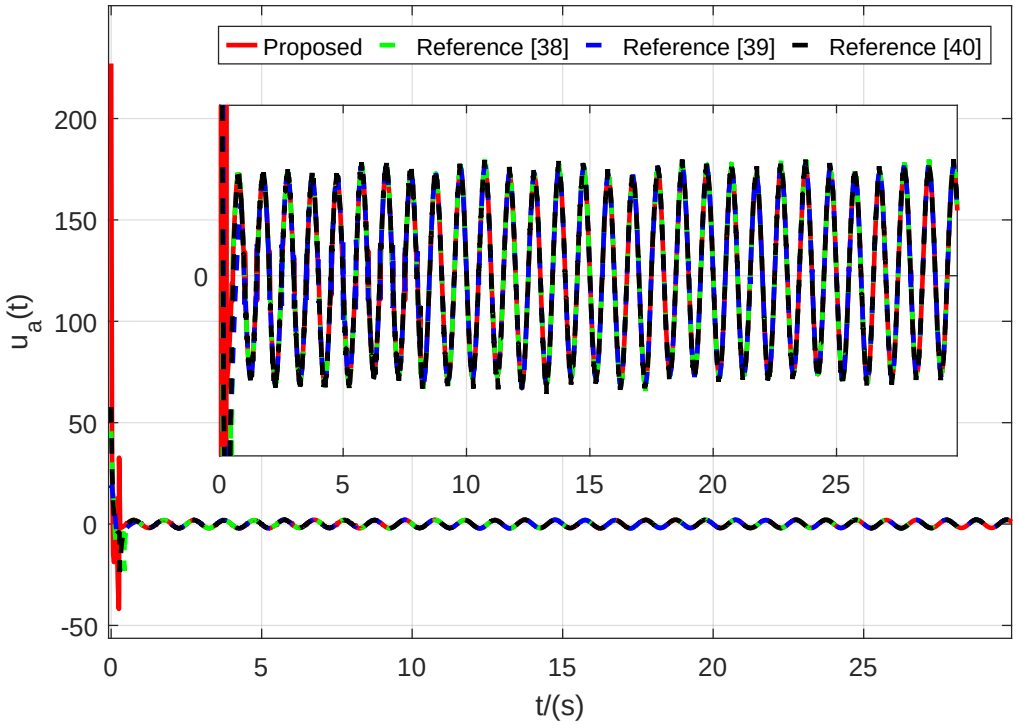


(a) Case 1

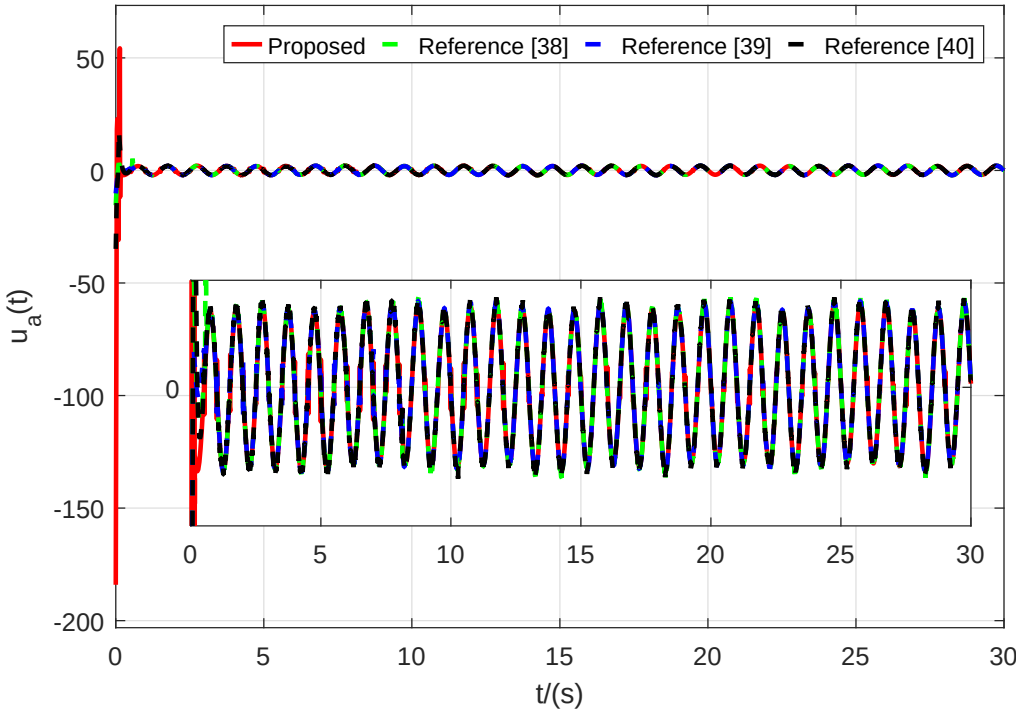


(b) Case 2

Figure 10. Sliding variable of the proposed controller for the Φ^6 Duffing oscillator.



(a) Case 1



(b) Case 2

Figure 11. Actual control input comparison for the Φ^6 Duffing oscillator.

4.2 Effectiveness of the ETM

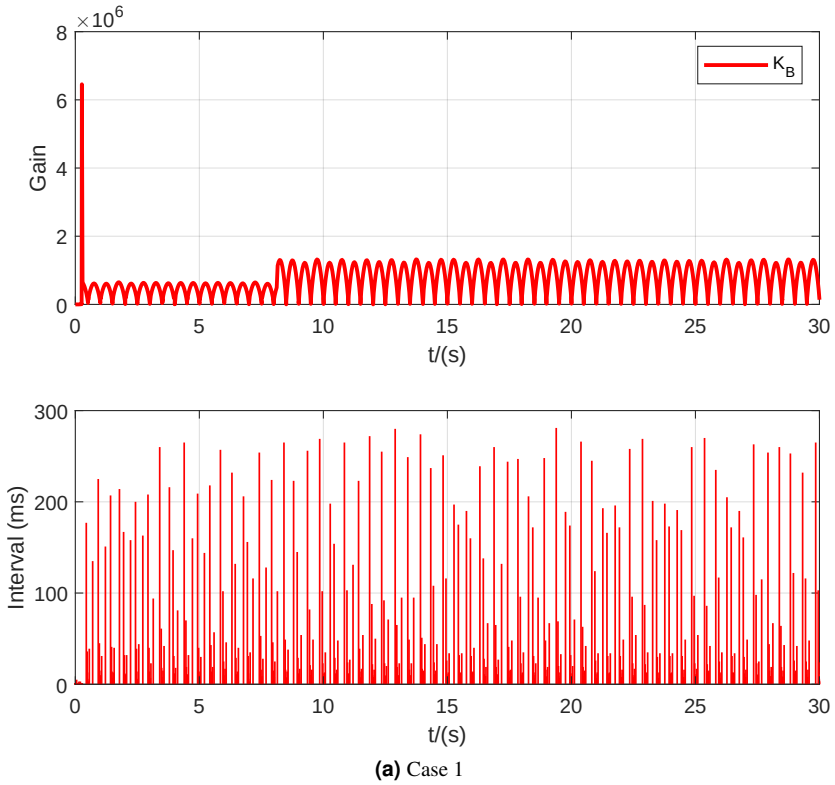
The communication performance of the proposed controller is evaluated using the number of nominal-command transmissions. With a checking period of $h = 0.001$ s, a periodic schedule contains 30000 transmission instants over $[0, 30)$ s. The percentage reduction is calculated as $(1 - N_{\mathrm{tr}}/30000) \times 100\%$, where N_{tr} is the number of nominal commands transmitted by the ETM.

Table 4 lists the transmission counts for the two oscillators. For the Duffing oscillator, 2046 and 2182 nominal commands are transmitted in Cases 1 and 2, corresponding to reductions of 93.18% and 92.73%. For the Φ^6 Duffing oscillator, the reductions are 93.23% and 92.74%, respectively. The ETM therefore reduces nominal-command transmissions by approximately 93% relative to the periodic schedule in all four tests.

Table 4. Communication performance

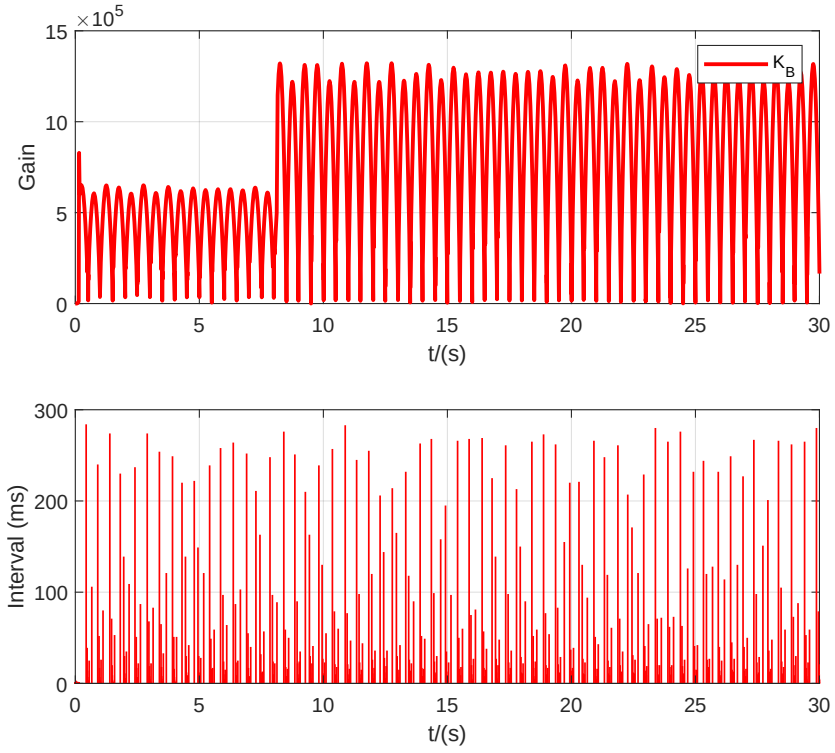
System	Case	Periodic schedule	Proposed	Reduction (%)
Duffing	1	30000	2046	93.18
Duffing	2	30000	2182	92.73
Φ^6 Duffing	1	30000	2031	93.23
Φ^6 Duffing	2	30000	2177	92.74

The barrier gains and inter-transmission intervals are shown in Figs. 12 and 13. The gains vary with the sliding variable, and the transmission intervals change during the transient and subsequent motion. Since transmission decisions are made on the checking grid, consecutive transmissions are separated by at least h. Together with the state trajectories and error responses, these results illustrate synchronization with fewer command transmissions.



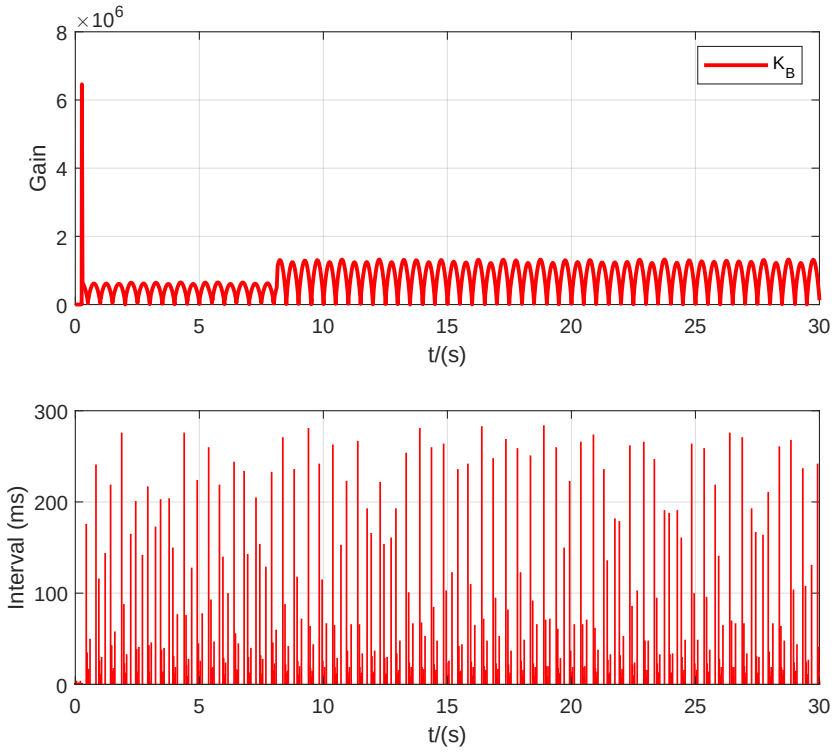
(a) Case 1

Figure 12. Barrier gains and inter-transmission intervals for the Duffing oscillator.



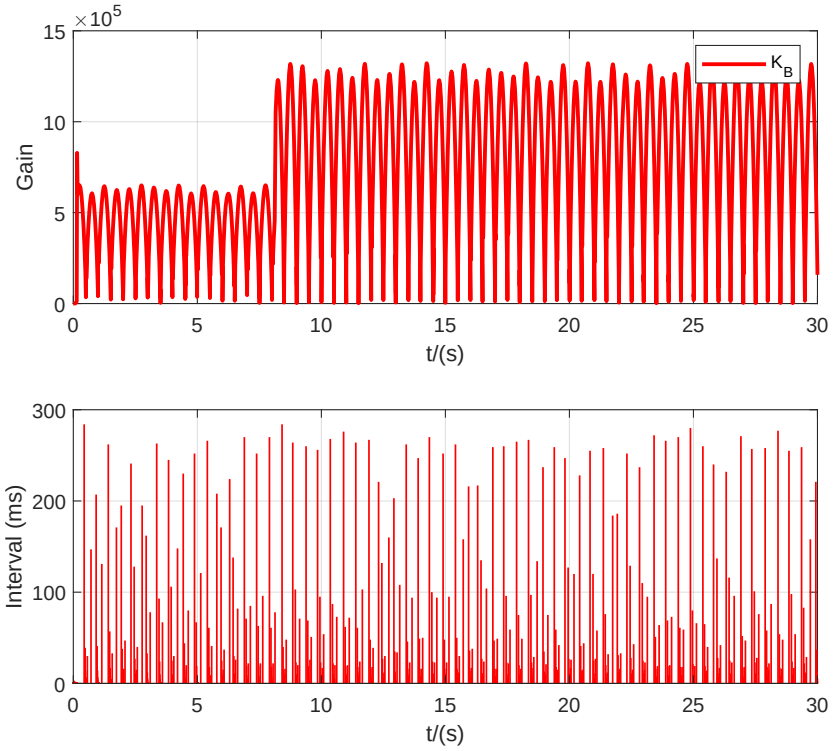
(b) Case 2

Figure 12. Barrier gains and inter-transmission intervals for the Duffing oscillator (continued).



(a) Case 1

Figure 13. Barrier gains and inter-transmission intervals for the Φ^6 Duffing oscillator.



(b) Case 2

Figure 13. Barrier gains and inter-transmission intervals for the Φ^6 Duffing oscillator (continued).

4.3 Additional tests under different prescribed durations

To further evaluate synchronization under different prescribed durations, the non-autonomous horizontal platform system in (5) is considered. The system parameters are selected as $b = 4/3$, $\lambda = 3.776$, $\mu = 4.6 \times 10^{-6}$, $\tau = 34/3$, and $\omega = 1.8$. Fig. 14 shows the phase trajectory with the initial state $(0.5, 0.5)$. The synchronization initial states are those of Case 1, and the same uncertainty, disturbance, and actuator fault are applied.

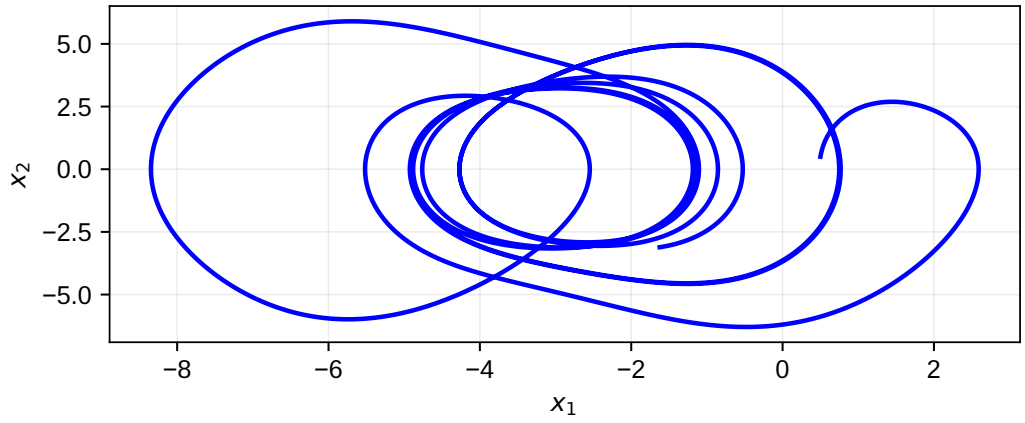


Figure 14. Phase trajectory of the non-autonomous horizontal platform system.

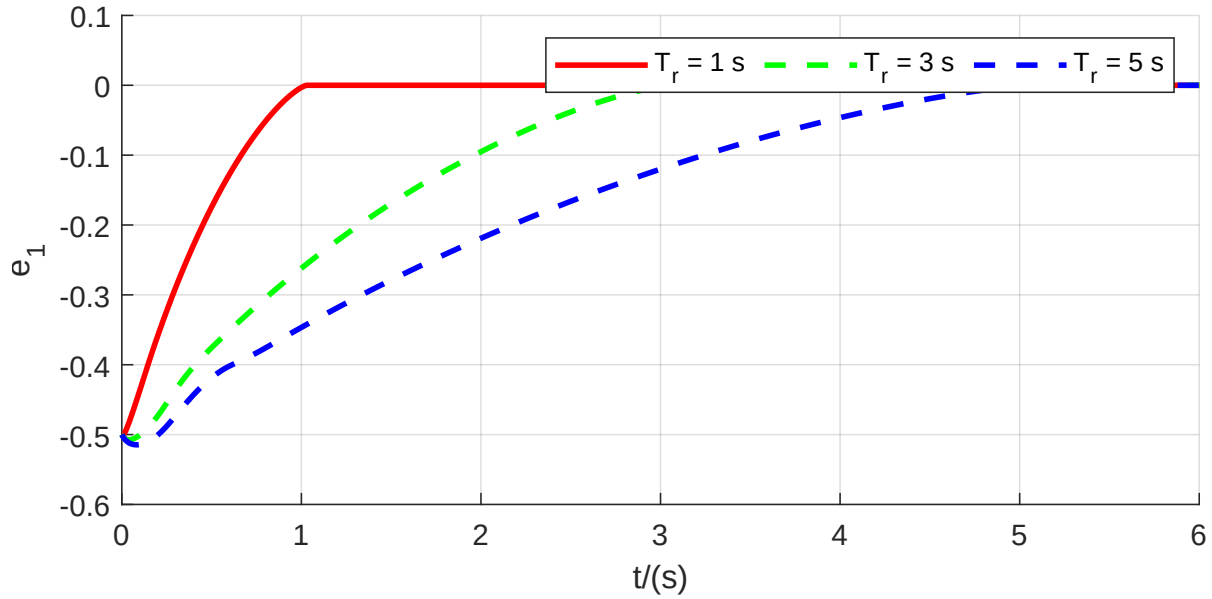
The time-scale parameter is selected as $T_r = 1$, 3, and 5 s, with $T_c = 2.793456T_r$ and $T_d = 0.171002T_r$. The remaining platform-controller parameters, supplied in the simulation files, are unchanged across these three runs. Table 5 gives the quantitative results. Both errors enter the tolerance band by 1.0298 s, 3.0578 s, and 5.0651 s, respectively, close to the selected durations.

The synchronization errors are depicted in Fig. 15. A shorter prescribed duration leads to a faster initial response and

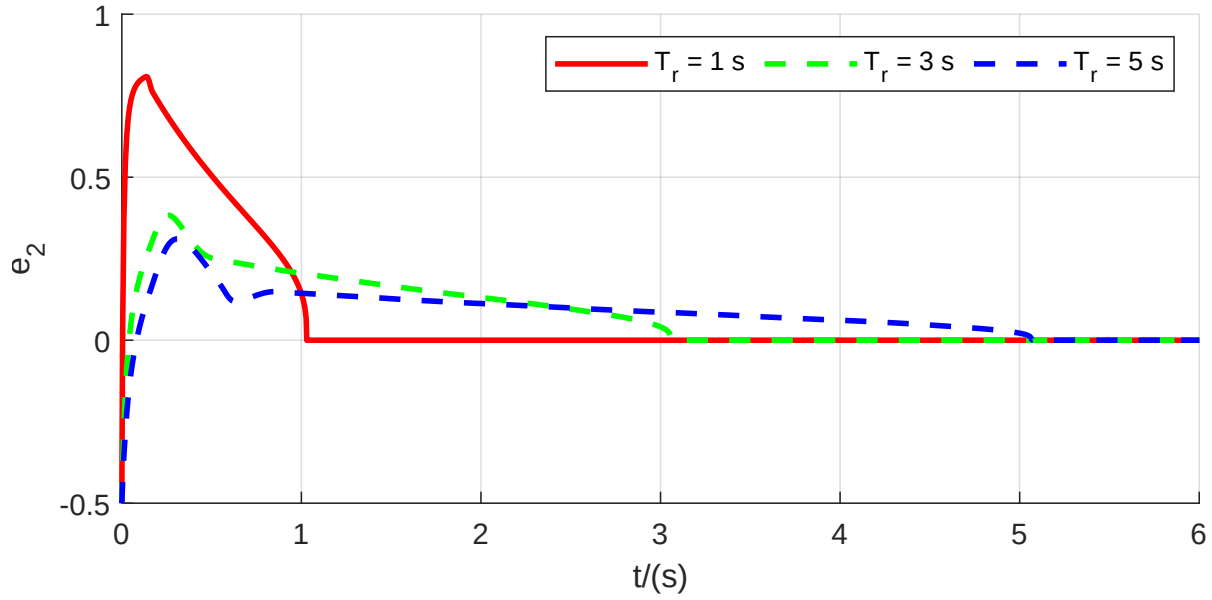
Table 5. Synchronization performance under different prescribed durations

Metric	$T_r = 1$ s	$T_r = 3$ s	$T_r = 5$ s
Convergence time of e_1 (s)	0.9879	2.9325	4.8562
Convergence time of e_2 (s)	1.0298	3.0578	5.0651
RMSE_1	0.0461	0.0791	0.1008
Peak actual control input	343.98	228.60	104.51

a smaller position-error RMSE. The peak actual input increases as the duration decreases. In particular, the sampled peak actual input increases from 104.51 at $T_r = 5$ s to 343.98 at $T_r = 1$ s. These results show how the selected duration affects synchronization speed, error evolution, and the required control input.



(a) Position error e_1



(b) Velocity error e_2

Figure 15. Synchronization errors under different prescribed durations.

5 Conclusions

This paper investigates the synchronization of second-order chaotic systems under uncertainties, external disturbances, actuator faults, and communication constraints using a predefined-time NTSMC strategy. An NTSMC is designed to achieve predefined-time convergence. To avoid gain mismatch, a time-varying barrier-function-based adaptive strategy is developed without requiring a priori knowledge of the disturbance upper bound. To reduce the communication burden, a periodic ETM is introduced. Numerical results show that the proposed controller achieves faster convergence, a smaller position-error RMSE, and reduced chattering, while the ETM reduces nominal-command transmissions by approximately 93%. The proposed scheme provides explicit control over convergence time and accuracy for high-precision chaotic synchronization under complex disturbances, actuator faults, and communication constraints. Future research focuses on experimental validation and practical secure-communication applications.

References

1. Q. Yao, Synchronization of second-order chaotic systems with uncertainties and disturbances using fixed-time adaptive sliding mode control, Chaos Solitons Fractals 142 (2021), 110372.
2. M. A. Sepestanaki, H. Rezaee, M. Soofi, H. Fayazi, S. H. Rouhani, and S. Mobayen, Adaptive continuous barrier function-based super-twisting global sliding mode stabilizer for chaotic supply chain systems, Chaos Solitons Fractals 182 (2024), 114828.
3. H. Zhang, X. Feng, J. Sun, and P. Yan, Chaotic Image Security Techniques and Developments: A Review, Mathematics 13(12) (2025), 1976.
4. W. Zheng, S. Qu, Q. Tang, and X. Du, Predefined-time sliding mode control for synchronization of uncertain hyperchaotic system and application, J. Vib. Control 31(3-4) (2025), 528–538.
5. S. Sahoo, R. Nathasarma, and B. K. Roy, Time-synchronized predefined-time synchronization between two non-identical chaotic systems, Chaos Solitons Fractals 181 (2024), 114662.
6. T. Tanze Wontchui, S. R. Ujjwal, D. S. Mbieda Petmegni, N. Punetha, M. Ekonde Sone, J. Y. Effa, and R. Ramaswamy, Multistability in chaotic coupled Lorenz systems near the Hopf bifurcation boundary: Emergence of new stable equilibria, Chaos Solitons Fractals 198 (2025), 116507.
7. J. Yang and Z. Jing, Inhibition of chaos in a pendulum equation, Chaos Solitons Fractals 35(4) (2008), 726–737.
8. X. Wu, J. Cai, and M. Wang, Global chaos synchronization of the parametrically excited Duffing oscillators by linear state error feedback control, Chaos Solitons Fractals 36(1) (2008), 121–128.
9. C.-C. Yang, Adaptive nonsingular terminal sliding mode control for synchronization of identical Φ^6 oscillators, Nonlinear Dyn. 69(1-2) (2012), 21–33.
10. M. P. Aghababa and H. P. Aghababa, Synchronization of mechanical horizontal platform systems in finite time, Appl. Math. Model. 36(10) (2012), 4579–4591.
11. M. Zhong, C. Huang, J. Cao, and H. Liu, Adaptive fuzzy echo state network optimal synchronization control of hybrid-order chaotic systems via reinforcement learning, Chaos Solitons Fractals 181 (2024), 114665.
12. Y. Mao, RBF Neural Network Fusion Disturbance Estimation for Robust Synchronization of Chaotic Systems, Mathematics 14(6) (2026), 1054.
13. H. Dong, C. Huang, J. Cao, and H. Liu, Adaptive fuzzy quantized prescribed performance synchronization of uncertain non-strict feedback chaotic systems with time-varying actuator failure, Inf. Sci. 681 (2024), 121241.
14. L. Zhao, X. Liu, and J. Jin, A novel adaptive parameter zeroing neural network for the synchronization of complex chaotic systems and its field programmable gate array implementation, Measurement 242 (2025), 115989.
15. Pallav, H. Handa, and B. B. Sharma, Sliding mode control based generalized technique for synchronization of identical and non-identical chaotic systems in presence of input nonlinearities, J. Vib. Control 32(9-10) (2026), 2461–2487.
16. S. Beyhan, An experimental set-up design for synchronization and control of coupled Hindmarsh–Rose neurons with Markov-jump dynamics: A case study on finite-time sliding-mode synchronization, Chaos Solitons Fractals 180 (2024), 114578.
17. H. Ding, J. Qian, D. Tian, and Y. Zeng, Norm-Based Adaptive Control with a Novel Practical Predefined-Time Sliding Mode for Chaotic System Synchronization, Mathematics 13(5) (2025), 748.

18. X. Tan and Y. Feng, A new pre-defined smooth mode control for chaotic synchronization with exponential function, Chaos Solitons Fractals 201 (2025), 117158.

19. E. A. Assali and R. Li, Laplace transform for a new adaptive predefined stability theorem and its application to the synchronization of chaotic systems, Chaos Solitons Fractals 199 (2025), 116778.

20. S. Yan, X. Wu, and J. Jiang, Dynamics analysis and predefined-time sliding mode synchronization of multi-scroll systems based on a single memristor model, Chaos Solitons Fractals 196 (2025), 116337.

21. Ö. Bingöl, Attitude synchronization of chaotic satellites with unknown dynamics using a neural network based fixed time sliding mode controller, Adv. Space Res. 75(3) (2025), 3242–3267.

22. Y. Lu and W. Yao, Active fault-tolerant hybrid control integrated with reinforcement learning application to cable-driven parallel robots, Control Eng. Pract. 158 (2025), 106277.

23. F. Ni, Y. Luo, J. Xu, D. Liu, Y. Sun, and W. Ji, Review of Fault-Tolerant Control Methods for Suspension Systems: From Road Vehicles to Maglev Trains, Mathematics 12(16) (2024), 2576.

24. J. Zhai and Y. Qin, Predefined-time adaptive fault tolerant anti-synchronization control for unified chaotic system with unknown actuator faults, Chaos Solitons Fractals 203 (2026), 117705.

25. Y. Shi, H. Yan, Y. Hu, M. Wang, and Z. Li, Predefined-time event-triggered sliding mode control of uncertain Euler-Lagrange dynamic systems with actuator faults, Int. J. Syst. Sci. 56(14) (2025), 3558–3570.

26. X. Cheng, M. Gao, L. Sheng, and Y. Wei, Fixed-time active fault-tolerant control for a class of nonlinear systems with intermittent faults and input saturation, J. Process Control 143 (2024), 103319.

27. Y. Chang, M. Hu, Z. Yang, Y. Bian, Z. Lei, and H. Qin, Active fault-tolerant path tracking control for autonomous vehicles considering actuator fault and model mismatch, Control Eng. Pract. 162 (2025), 106362.

28. N. Shao, S. Wu, Y. Xie, L. Liu, and Y. Fang, Predefined-Time Prescribed Performance Fault-Tolerant Control for a Class of Uncertain Nonlinear Systems Under Full State Constraints, Int. J. Adapt. Control Signal Process. 39(6) (2025), 1335–1350.

29. C. Yin, Z. Zhao, and P. Yi, Sliding mode fault-tolerant control for manipulator based on predefined time extended state observers, ISA Trans. 168 (2026), 236–246.

30. S. Rafiee, M. Kankashvar, P. Mohammadi, and H. Bolandi, Active fault-tolerant attitude control based on Q-learning for rigid spacecraft with actuator faults, Adv. Space Res. 74(3) (2024), 1261–1275.

31. X. Ren, Q. Guo, X. Dai, and T. Li, Adaptive Fixed-Time Fault-Tolerant Control for Robotic Manipulators With Actuator Loss of Effectiveness Faults and Unknown Nonlinearities, Int. J. Robust Nonlinear Control 35(17) (2025), 7337–7354.

32. M. Mazare, M. Taghizadeh, P. Ghaf-Ghanbari, and E. Davoodi, Robust fault detection and adaptive fixed-time fault-tolerant control for quadrotor UAVs, Robot. Auton. Syst. 179 (2024), 104747.

33. J. Ma, H. Zhang, J. Zhang, and L. Wang, Event-based predefined-time anti-synchronization for unified chaotic systems and the application to Chua's circuit, Chaos Solitons Fractals 188 (2024), 115534.

34. Y. Yan, S. Yu, X. Gao, D. Wu, and T. Li, Continuous and Periodic Event-Triggered Sliding-Mode Control for Path Following of Underactuated Surface Vehicles, IEEE Trans. Cybern. 54(1) (2024), 449–461.

35. Y. Yan, T. Jin, X. Yu, S. Yu, and G. Guo, Event-Triggered Nonsingular Terminal Sliding-Mode Control, IEEE Trans. Cybern. 55(7) (2025), 3356–3367.

36. Y. Gao, Y. Zhao, L. Wen, S. Yu, and H. Sang, Event-triggered sliding mode control for uncertain systems with multiple disturbances, Int. J. Syst. Sci. 55(10) (2024), 2131–2143.

37. A. K. Behera, Event-triggered sliding mode control via digital redesign, Automatica 177 (2025), 112349.

38. S. Mobayen, B. Vaseghi, J. Zhang, J. Ma, Q. Zhu, and A. Fekih, Adaptive nonsingular barrier function-based terminal sliding mode control for disturbed nonlinear systems with application to chaos-based secure communication, J. Vib. Control (2025), first published online 20 September 2025.

39. H. Sai, Z. Xu, and J. Cui, Nonconservative adaptive practical predefined-time sliding mode tracking of uncertain robotic manipulators, Int. J. Robust Nonlinear Control 33(18) (2023), 11036–11061.

40. A. Sarjaš and D. Gleich, Barrier Function Adaptive Event-Triggered Sliding Mode Control for Nonlinear Systems, Mathematics 14(16) (2026), 2882.

41. Y. Sun, Y. Gao, Y. Zhao, Z. Liu, J. Wang, J. Kuang, F. Yan, and J. Liu, Neural Network-Based Tracking Control of Uncertain Robotic Systems: Predefined-Time Nonsingular Terminal Sliding-Mode Approach, IEEE Trans. Ind. Electron. 69(10) (2022), 10510–10520.

Author contributions statement

This study was successfully completed through the collaborative efforts of all the authors. Xinxin Zhuang was responsible for conceptualizing the study, developing the methodology, conducting the formal analysis, and preparing the initial manuscript. Wentao Qin contributed to the methodological design, implemented the software, performed the simulations and validation, and reviewed and revised the manuscript. An Yan contributed to the formal analysis, investigation, validation, and visualization, and participated in reviewing and editing the manuscript. Huikun Hao contributed to reviewing and revising the manuscript to improve its clarity and accuracy. All authors have read and approved the final version of the manuscript for publication.

Data Availability Statement

All data generated or analysed during this study are included in this published article.

Competing interests

The authors declare no competing interests.

Corresponding author

Correspondence to Xinxin Zhuang.

Funding

This work was supported in part by the Training of Professionals in Smart Healthcare and Elderly Care at the Primary Care Level under Grant JNSX2025062 and the Shandong Provincial Natural Science Foundation under Grant ZR2024QE335.